

**ANNALS OF THE UNIVERSITY OF CRAIOVA**

**Series: AUTOMATION, COMPUTERS, ELECTRONICS AND MECHATRONICS**

**Vol. 13 (40), No. 1, 2016**

**ISSN 1841-0626**

**Note:** The “Automation, Computers, Electronics and Mechatronics Series” emerged from “Electrical Engineering Series” (ISSN 1223-530X) in 2004.

**Honorary Editor:**

Vladimir RĂSVAN – University of Craiova, Romania

**Editor-in-Chief:**

Liana STĂNESCU – University of Craiova, Romania

**Associate Editors-in-Chief:**

Marius BREZOVAN – University of Craiova, Romania

Dorian COJOCARU – University of Craiova, Romania

Dan SELIȘTEANU – University of Craiova, Romania

**Editorial Board:**

Costin BĂDICĂ	– University of Craiova, Romania
Andrzej BARTOSZEWICZ	– Institute of Automatic Control, Technical University of Lodz, Poland
Nicu BÎZDOACĂ	– University of Craiova, Romania
David CAMACHO	– Universidad Autonoma de Madrid, Spain
Kazimierz CHOROS	– Wrocław University of Technology, Poland
Ileana HAMBURG	– Institute for Work and Technology, FH Gelsenkirchen, Germany
Mirjana IVANOVIC	– University of Novi Sad, Serbia
Mircea IVĂNESCU	– University of Craiova, Romania
Vladimir KHARITONOV	– University of St. Petersburg, Russia
Peter KOPACEK	– Institute of Handling Device and Robotics, Vienna University of Technology, Austria
Rogelio LOZANO	– CNRS – HEUDIASYC, France
Dan Bogdan MARGHITU	– Auburn University, Alabama, USA
Marius MARIAN	– University of Craiova, Romania
Mihai MOCANU	– University of Craiova, Romania
Sabine MONDIÉ	– CINVESTAV (Department of Automatic Control), Mexico
Ileana NICOLAE	– University of Craiova, Romania
Silviu NICULESCU	– CNRS – SUPELEC (L2S), France
Mircea NIȚULESCU	– University of Craiova, Romania
Sorin OLARU	– CNRS – SUPELEC (Automatic Control Department), France
Octavian PASTRAVANU	– “Gheorghe Asachi” Technical University of Iasi, Romania
Emil PETRE	– University of Craiova, Romania
Dan PITICĂ	– Technical University of Cluj-Napoca, Romania
Dan POPESCU	– University of Craiova, Romania
Elvira POPESCU	– University of Craiova
Radu-Emil PRECUP	– “Politehnica” University of Timisoara, Romania
Dorina PURCARU	– University of Craiova, Romania
Monica ROMAN	– University of Craiova
Dan STOIANOVICI	– Johns Hopkins University, Baltimore, Maryland, USA
Dorin ȘENDRESCU	– University of Craiova
Sihem TEBBANI	– CNRS – SUPELEC (Automatic Control Department), France

**Editorial Secretary :** Lucian BĂRBULESCU – University of Craiova, Romania

**Address for correspondence:** Liana STĂNESCU

University of Craiova, Faculty of Automation, Computers and Electronics

Al.I. Cuza Street, No. 13, RO-200585, Craiova, Romania

Phone: +40-251-438198, Fax: +40-251-438198

Email: stanescu@software.ucv.ro

**We exchange publications with similar institutions from country and from abroad**



## CONTENTS

Dorina PURCARU, Anca PURCARU: <i>Experimental Systems for Acquiring Technical Knowledge and Practical Skills on Electronic Measurements</i>	5
Lavinu Aurelian BĂDULESCU: <i>Pruning Methods and Splitting Criteria for Optimal Decision Trees Algorithms</i>	15
Faiq BAJI, Mihai MOCANU: <i>Diagnosis Melanoma Skin Cancer Using ABCD Rule, Statistic Texture Feature and Lesion Symptoms</i>	20
Traian-Titi ȘERBAN: <i>Temperature Data Logger for Industrial and Environmental Monitoring</i>	28
George Cristian CĂLUGARU, Ionuț Cristian RESCEANU, Elena Andreea DĂNIȘOR: <i>Constrained Optimal Control and Feasibility Studies Performed for Landing Aircraft</i>	34
Viorel Costin BANȚA, Dorian COJOCARU: <i>Integration of metrology principles in the next generation of ERP using SAP Fiori interface, collaboration, SaaS and SOA</i>	40
Author Index	49



## Experimental Systems for Acquiring Technical Knowledge and Practical Skills on Electronic Measurements

Dorina Purcaru\*, Anca Purcaru\*\*

\* *Department of Automation and Electronics, University of Craiova  
Craiova, Romania (e-mail: dpurcaru@electronics.ucv.ro).*

\*\**VIG IMPEX  
Craiova, Romania (e-mail: aipurcaru@gmail.com).*

---

**Abstract:** An efficient training in the measurement systems field requires theoretical knowledge and practical skills in using sensors, transducers, electronic devices and circuits. The paper presents a guideline for thorough understanding the operation and programming of inductive, capacitive and ultrasonic sensors, resistance temperature detector and intelligent temperature sensor. The information from user manuals and datasheets is selected, explained and completed with suggestive graphic representations and static transfer characteristics. Three experimental systems allow the sensors' testing and monitoring and implement a temperature control system and a motion control system. The sensor monitoring and remote programming and the applications' implementation require a programmable logic controller. These experimental systems have been proved very useful in academic study for experimental training on measurement systems.

*Keywords:* education, sensors, monitoring, testing, programmable logic controller, programs.

---

### 1. INTRODUCTION

The education in measurement and instrumentation has been a concern for more researchers over the past few years; among these may be mentioned (Frota et al., 2006, 2013), (Olowokere, 2015), (Koch et al., 2017), and (Purcaru et al., 2009a). Experimental systems are very useful for engineering education in Electronics and Measurement systems; such systems were presented in (Purcaru, 1998), (Purcaru et al., 2000, 2009b, 2011), and (Ibrahim, 2015) easing the students' learning process.

The paper presents a guideline for studying more sensors and three experimental systems that implement applications of these devices. The engineering undergraduates acquire technical knowledge and practical skills using inductive, capacitive and ultrasonic sensors, resistance temperature detector and intelligent temperature sensor. The sensors' applications are implemented using a programmable logic controller (Özerdem, 2016). The programs loaded on this programmable logic controller allow the sensor monitoring and programming, implementing an on-off temperature control system and a motion control system.

### 2. UNDERSTANDING THE OPERATING AND PROGRAMMING OF STUDIED SENSORS

#### 2.1 Sensor Output Function and Type

Each studied sensor has an analogue or switching (digital) output (Catalog, 2011, 2014). The signal provided from the analogue output is current or voltage type and it

depends on the physical quantity measured by the sensor; this dependence is usually linear.

The output function is *normally open (NO) contact* or *normally closed (NC) contact* at each switching output (Catalog, 2015), the contact being implemented with a bipolar transistor at the sensor output. The *NO contact* function means that the output voltage is high and the output transistor is *on* (closed contact) when the sensor is activated. The *NO contact* function meets the situation of high output voltage and *on* output transistor (closed contact) when the sensor is activated. The *NC contact* function notifies that the output voltage is low and the output transistor is *off* (open contact) when the sensor is activated.

The output function and type of the studied sensors are presented below.

The intelligent temperature sensor has two outputs: the first is switching and the second can be programmed as switching or analogue (current). The output function of each switching output is programmable (*NO contact* or *NC contact*).

The ultrasonic, inductive and capacitive proximity sensors have switching outputs. The output function is *NO contact* for all sensors excepting the intelligent ultrasonic sensor, which provides a programmable output (*NO contact* or *NC contact*).

#### 2.2 Intelligent Temperature Sensor Operation and Programming

A studied intelligent temperature transducer consists of the TP-203A-CF-H1141-L100 resistance temperature detector connected to the TS-500-LI2UPN8X-H1141 intelligent sensor. The resistance temperature detector is a Pt100 probe with  $-30...350^{\circ}\text{C}$  temperature range (Datasheet, 2015). The intelligent temperature sensor of the TS500 series is a processing unit with a 4-digit, 7-segment display, two outputs and a PNP transistor at each switching output (User manual, 2012, 2016). This device processes signals from a resistance temperature detector or thermowell. The status of each switching output is displayed with a yellow LED which lights when the output transistor is *on*.

The intelligent temperature transducer has two switching functions: *Hysteresis* and *Window*. The diagrams from Fig. 1- 4 graphically explain the two switching functions. These diagrams were obtained by completing and detailing the graphical representations from (User manual, 2012, 2016) and (Purcaru, 2012) for *Hysteresis* and *Window* functions.

The *Hysteresis* function ensures a stable switching status around the adjusted set point, independent of the system inherent temperature fluctuations. There can be two situations: *Hysteresis with NO operation* (acronym *Hno* in (User manual, 2012)) and *Hysteresis with NC operation* (acronym *Hnc* in (User manual, 2012)), respectively. The yellow LED status,  $U_o$  output voltage level, output contact and  $Q_s$  transistor status are all specified in Fig. 1 with the  $T$  temperature rising and decreasing. The user sets the switching range through a *switch point (SP)* and a *reset point (rP)*; the notations are the same as in (User manual, 2012).

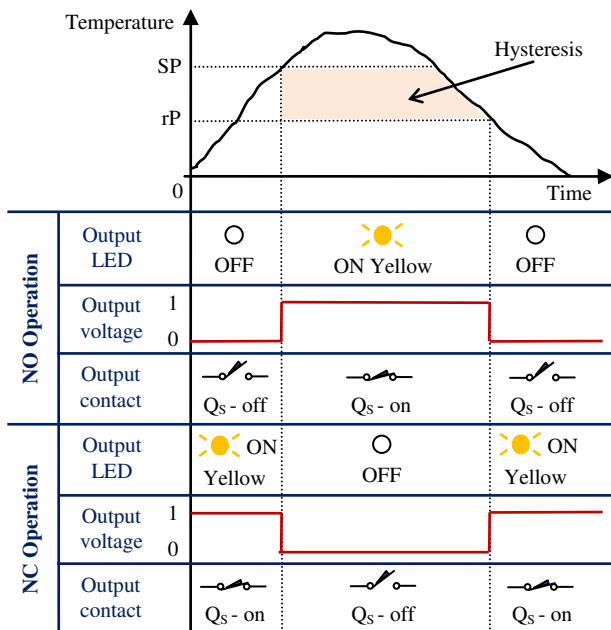


Fig. 1. Output status and signalling of intelligent temperature transducer for *Hysteresis* switching function.

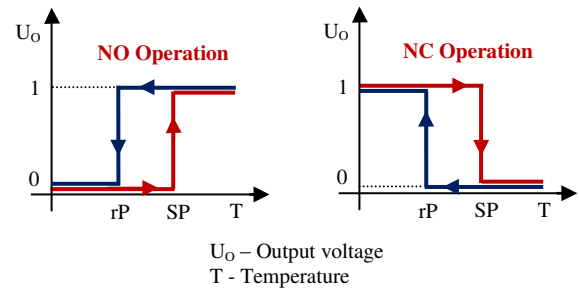


Fig. 2. The static transfer characteristics of the intelligent temperature transducer for *Hysteresis* switching function.

The graphical representation from Fig. 1 allows the thorough understanding of intelligent temperature transducer operating in all situations for *Hysteresis* function, and the correspondence between  $U_o$  voltage level,  $Q_s$  output transistor, output contact and yellow LED status at the switching output.

The static transfer characteristic ( $U_o$  output voltage versus  $T$  temperature) of the studied temperature transducer for *Hysteresis* function is drawn in Fig. 2 based on the graphical representation from Fig. 1. The transfer characteristic is travelled on a path to temperature increasing and on another path to temperature decreasing. The two paths are marked with different color and arrows. This characteristic clearly highlights the hysteresis and the engineering undergraduates can observe the similarity with the static transfer characteristic (output voltage versus input voltage) of voltage comparators with hysteresis, studied to Electronics. The *Window* function (User manual, 2012, 2016) provides a temperature range in which the sensor's output switch assumes a defined status (Fig. 3).

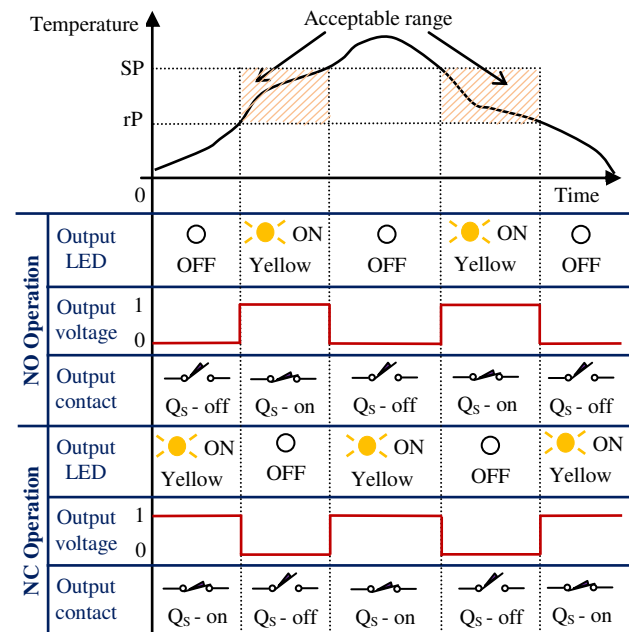


Fig. 3. Output status and signalling of intelligent temperature transducer for *Window* switching function.

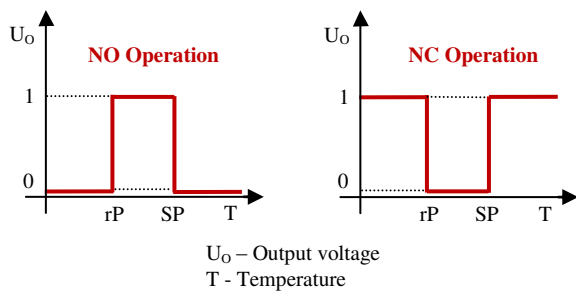


Fig. 4. The static transfer characteristics of the intelligent temperature transducer for *Window* switching function.

The user defines this range by setting an *upper window limit* ( $SP$ ) and a *lower window limit* ( $rP$ ) specified in Fig. 3 and 4. The  $T$  temperature versus time, the corresponding  $U_o$  output voltage versus time and the status of yellow LED, output contact and  $Q_s$  transistor can be seen in Fig. 3. The analysed situations are the following: *Window* function with *NO operation* (acronym *Fno* in (User manual, 2012)), and *Window* function with *NC operation* (acronym *Fnc* in (User manual, 2012)). The corresponding static transfer characteristics  $U_o=f(T)$  of the studied temperature transducer for *Window* switching function are shown in Fig. 4, based on the graphical representation from Fig. 3, for NO and NC operation. The absence of hysteresis is observed.

The second output of the intelligent temperature sensor can be programmed as analogue. In this situation, the transducer's output current depends linearly on temperature in the measuring range.

Additional external devices (for example laptop) are not required for the intelligent temperature sensor programming. With the menu structure presented in (User manual, 2012) it is possible to set the output function, the values for the setting points, the range of analogue output current, increasing or decreasing transfer characteristic and many special functions such as switch delays or display rotation by  $180^\circ$ .

The temperature sensors of the TS500 series can be easily programmed with three push buttons: *Mode*, *Set*, and *Enter*. The *Mode* and *Set* buttons can be used to select and set different parameters; these buttons can be operated with fingers without tools. It is possible to scroll up and down through the values for improved operation. If the set value is to be saved and the programming is to be changed, the *Enter* button must be pressed. This button is recessed in order to avoid unintentional modification of the data stored in the sensor. Only after a tool is used can the operator permanently modify the sensor setting.

### 2.3 Ultrasonic Sensors Operating and Programming

The ultrasonic sensor emits a sound pulse that reflects off of an object entering the wave field. The reflected sound is then received by the sensor and it generates an analogue or digital output signal (Catalog, 2005, 2016). Ultrasonic sensing technology is based on the principle that sound

has a relatively constant velocity. The time for an ultrasonic sensor's beam to strike the target and return is directly proportional to the distance from the object (Busslinger, 2001). Ultrasonic sensors are capable of detecting most objects (metal or non-metal, clear or opaque, liquid, solid, or granular) that have sufficient acoustic reflectivity. The basic components of each ultrasonic sensor are transducer/receiver, comparator, detector circuit, and output circuit (Yousefimanesh, 2012). The signal from digital sensor indicates the presence or absence of an object in the sensing field, and the signal from analogue sensor indicates the distance to an object in the sensing field. Some typical applications are presented in (Catalog, 2016) and (User manual, 2013).

The sound cone of ultrasonic sensor - shown in Fig. 5 - contains the following characteristic zones:

- blind zone (unusable area, dead zone) – the object positioned in this zone cannot be detected;
- sensing range (operating range) – the object positioned in this zone can be detected;
- detection zone (measuring interval, switching interval) – the object positioned in this zone is detected.

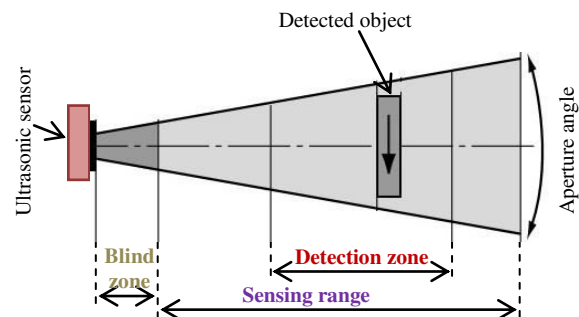


Fig. 5. The sound cone of ultrasonic sensor.

One of the experimental systems presented in this paper allows the study of two ultrasonic sensors: a diffuse mode sensor (RU30-Q30-AP8X-H1141) and a miniature ultrasonic sensor with Teach-mode programming (QS18UPA). Each sensor has a switching output and the output contact is implemented with a PNP transistor. The output function is programmable for QS18UPA and *NO contact* for RU30 only. The switching output is *window mode* with *switching hysteresis* for both studied ultrasonic sensors. Using the specifications from (User manual, 2007) and (Datasheet, 2010, 2016) we have drawn the static transfer characteristics ( $U_o$  output voltage versus  $d$  distance to target) shown in Fig. 6 and 7 for NO and NC operation. We denoted with  $A$  and  $B$  the lower limit and upper limit of the detection zone; each limit has two values ( $A_1, A_2$ , and  $B_1, B_2$ , respectively) due to hysteresis. The transfer characteristic is travelled on a path when the object approaches the sensor and on another path when the object moves away from the sensor; the two paths are marked with different color and arrows. The running

mode of studied ultrasonic sensors can be better understood from these static transfer characteristics.

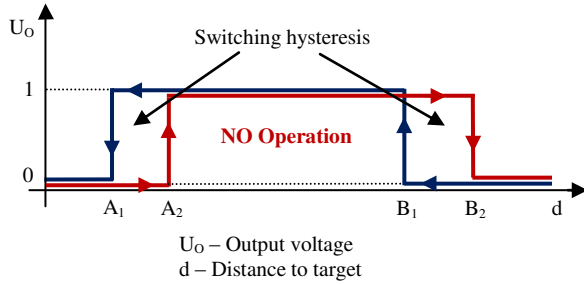


Fig. 6. The static transfer characteristic of ultrasonic sensor for *window mode*, *switching hysteresis* and normally open operation.

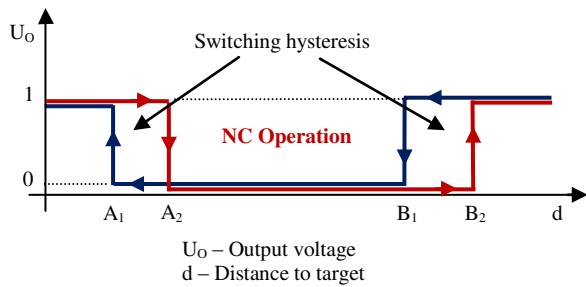


Fig. 7. The static transfer characteristic of ultrasonic sensor for *window mode*, *switching hysteresis* and normally closed operation.

QS18UPA sensor may be programmed either via its push button, or via a remote switch. The output function (*NO contact* or *NC contact*) can be changed and the push button can be disabled by remote programming only (User manual, 2007). The two *Teach* methods for local or remote programming of QS18 ultrasonic sensor (Datasheet, 2010) are the following:

- teach individual lower limit and upper limit of the detection zone;
- use *Auto-Window* feature to center a detection window around the taught position; the window width is 20 mm.

The output status and signalling of QS18UPA ultrasonic sensor during its operation are clearly highlighted in Fig. 8. The Power LED indicates the sensor status: it lights green (if target is within sensing range), red (if target is weak or outside sensing range) or it is *off* (if the sensor power supply is *off*). The Output/Teach LED lights yellow (when target is within taught limits of the detection zone), red (solid or flashing, when the sensor is in *Teach* mode) or it is *off* (when target is outside taught limits of the detection zone or the sensor power supply is *off*). The engineering undergraduates can observe the correspondence between the  $U_o$  output voltage level,  $Q_s$  output transistor, output contact and bi-color LED statuses at the switching output.

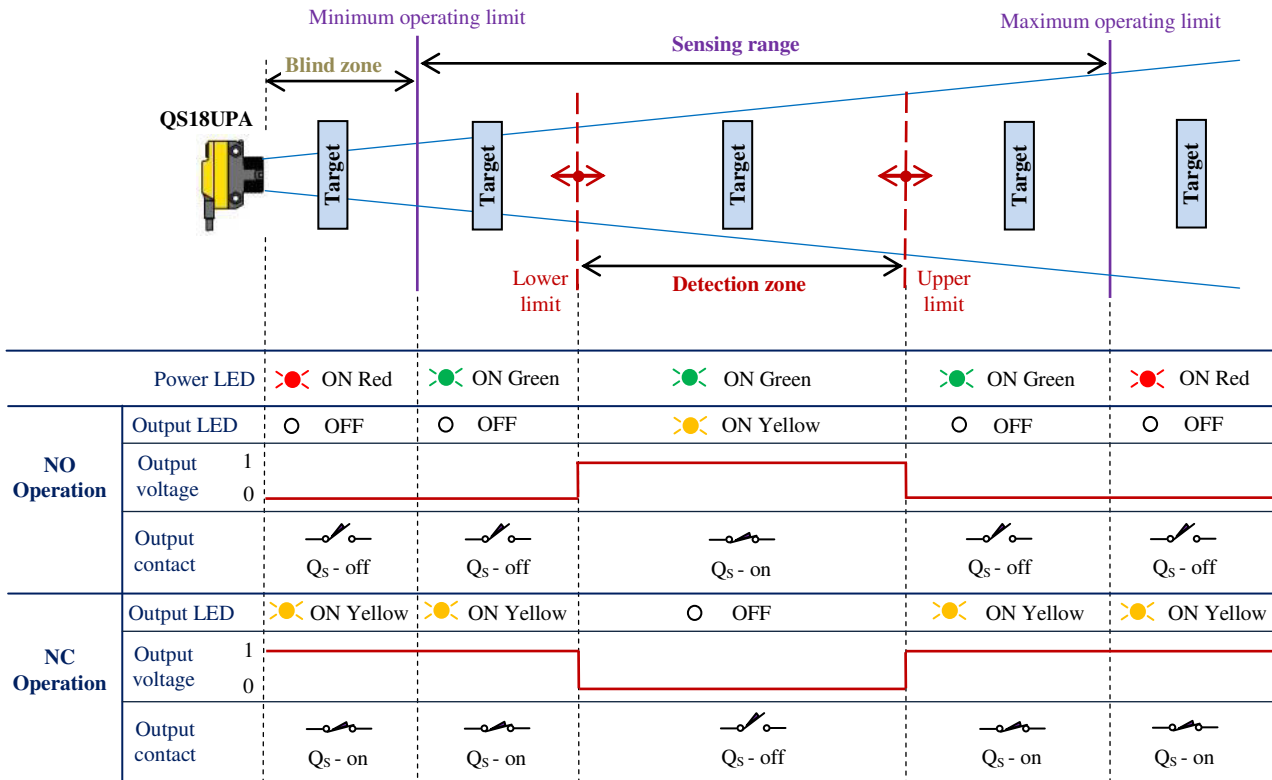


Fig. 8. Output status and signalling of QS18UPA ultrasonic sensor.



The output status and signalling of RU30 ultrasonic sensor during its operation are clearly depicted in Fig. 9. Only the upper limit of detection zone is adjustable via potentiometer (Datasheet, 2016); the near limit is determined by the blind zone. The output LED lights strong yellow (if target is within the limits of the detection zone), yellow (if the sensor power supply is on), and it is off (if the sensor power supply is off). By analyzing Fig. 9, the engineering undergraduates understand the running mode of this ultrasonic sensor better.

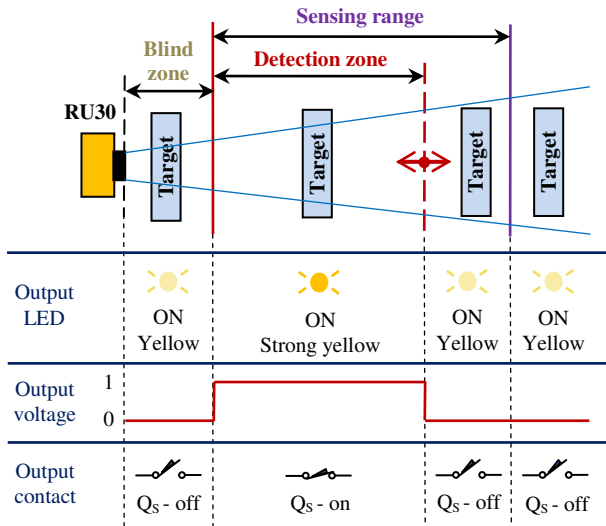


Fig. 9. Output status and signalling of RU30 ultrasonic sensor.

#### 2.4 Inductive and Capacitive Proximity Sensors Operating

The output function is *NO contact* and a PNP transistor implements this contact for both studied proximity sensors: inductive (Ni4U-Q8SE-AP6X-V1131) and capacitive (BC3-M12-AP6X). So,  $Q_S$  output transistor is on,  $U_O$  output voltage is high and a yellow LED lights when the target is within the limits of the detection zone. Fig. 10 clearly presents the running way of inductive or capacitive proximity sensor (Purcaru et al., 2017b). We have drawn this figure based on the specifications from (Catalog, 2012, 2015) and (Datasheet, 2017a, 2017b). The students can comprehend the connection between  $d$  distance from the sensor to the target and the level of  $U_O$  output voltage,  $Q_S$  transistor status, output contact status and yellow LED status. The proximity sensor acts like a closed contact when it detects an object in the detection zone.

The switching function is *Hysteresis* for both studied proximity sensor. The sensor behaviour when the target approaches or leaves the sensor face is detailed in Fig. 10. The sensor output switches in high level when the target approaches the sensor face and reaches the *operate point* ( $A_1$  distance in Fig. 10). The sensor returns to its normal state (low level of output voltage) when the target reaches the *release point* ( $A_2$  distance in Fig. 10). So, the sensing distance is delimited by the thresholds  $A_1$  and  $A_2$ .

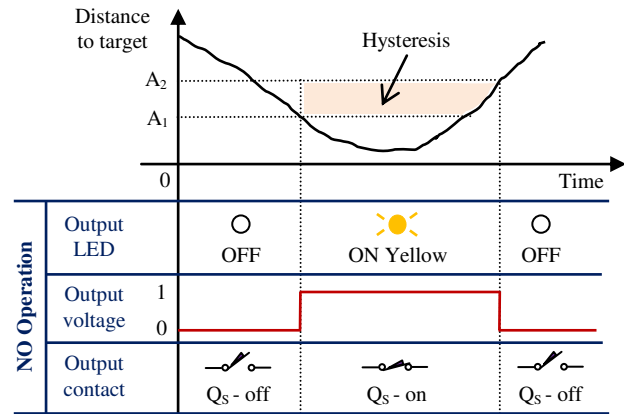


Fig. 10. Output status and signalling of Ni4U and BC3 proximity sensors.

The *hysteresis* or *differential travel* is the dissimilarity between *operate* and *release* points. The hysteresis is factory set at less than 15% (for inductive sensor) or 20% (for capacitive sensor) of the effective operating distance (Catalog, 2012, 2015). The hysteresis is needed in many of the proximity sensor applications (Catalog, 2012, 2015).

The static transfer characteristic ( $U_O$  output voltage versus  $d$  distance to target) of the studied inductive and capacitive proximity sensors is depicted in Fig. 11.b, based on the graphical representation from Fig. 10; the hysteresis is highlighted as in Fig. 2, 4, 6 and 7.

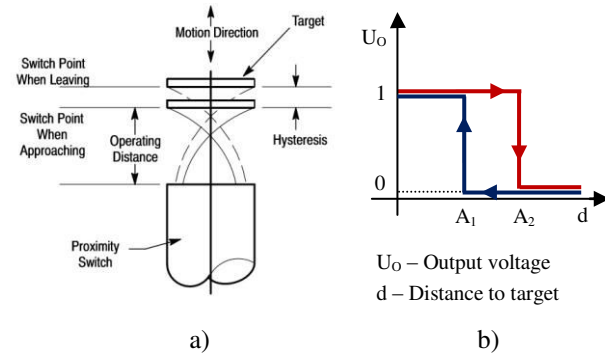


Fig. 11. Hysteresis function for Ni4U and BC3 proximity sensors: a) Functional principle. b) Static transfer characteristic.

The deduction of the sensor static transfer characteristic makes the correlation between sensor information (Catalog, 2012, 2015) and the knowledge gathered at Electronics and System theory possible.

### 3. TESTING, MONITORING AND APPLICATIONS OF SEVERAL SENSORS

Three experimental systems perform the testing and monitoring of the above presented sensors and the implementation of some simple applications. A programmable logic controller (PLC) allows the sensor remote programming, monitoring and applications' implementation (Purcaru, 2012).

The PLC process control equipment is organized around a microcontroller and it is keyboard, display and interface featured. PLC-03 has 8 digital inputs and 8 digital open collector outputs. Both digital input and output channels have galvanic isolation implemented with optocouplers.

A 24Vdc industrial power supply of the MDR-20 series (Datasheet, 2007) is used both for sensors and auxiliary devices and circuits required for the sensor study or for implemented applications.

The main benefits of using these experimental systems are the following:

the undergraduates are getting to understand and use theoretical knowledge previously acquired at Electronic devices and circuits, Measurement systems, Sensors and transducers, System theory, Programmable logic controllers, Data acquisition systems;

the users acquire practical skills working with real sensors and transducers, programmable logic controller, power supply and other devices and circuits;

the engineering undergraduates thoroughly understand the sensors' operating and programming using the explanations, diagrams and static transfer characteristics above presented;

the students can observe, measure and compare the hysteresis of inductive, capacitive and ultrasonic proximity sensors;

the undergraduates learn to design and implement an on-off temperature control system and a motion control system.

### 3.1 Monitoring the Sensor Switching Output

Each sensor switching output can be monitored using the programmable logic controller; the sensor connection to PLC is shown in Fig. 12. The equivalent circuit and wiring diagram of the switching output (shown in Fig. 12) are the same for each studied sensor (Purcaru, 2012).

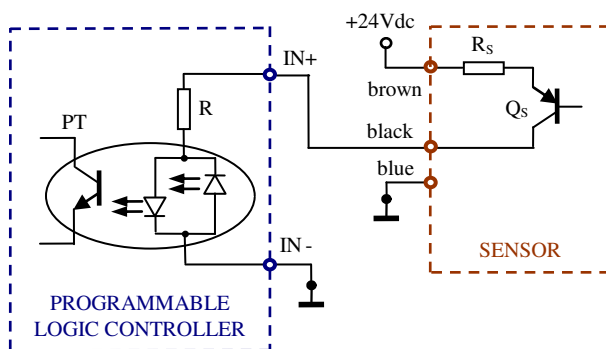


Fig. 12. The sensor connection to the programmable logic controller for monitoring the sensor switching output.

The collector of sensor's  $Q_s$  output transistor is connected to one of the two terminals of the selected input of PLC. An optocoupler provides the electrical isolation between PLC input and sensor output.

Students will supply the PLC and the monitored sensor. A program which allows displaying the switching output status of monitored sensor is loaded onto PLC. When  $Q_s$  transistor is *on*, the *PT* phototransistor is also *on* and PLC displays *0*. Otherwise, the displayed digit is *1*. If the output function is *NO contact*, digit *0* displaying on PLC means the sensor's activation (e.g. the presence of a target in the proximity sensor's detection zone), and digit *1* displaying means inactivated sensor. Hence, PLC displays *0* when the output LED of proximity sensor lights yellow (for Ni4U, BC3, QS18) or strong yellow (for RU30). If the output function is *NC contact*, digit *1* displaying on PLC signals the sensor's activation. A remote monitoring of sensor switching output is this way implemented.

The programmable logic controller allows both single-ended and fully-differential input voltage because the two terminals of the input circuit. The optocoupler with two LEDs connected in anti-parallel allows reversed polarity of input voltage. A detailed analysis of the circuit from Fig. 12 helps students to better understand the sensor connection to PLC, to assess whether the two devices are compatible, and to acquire practical skills for such connections.

### 3.2 Experimental System for Testing an Intelligent Temperature Transducer and Implementing an on-off Temperature Control

The experimental system that allows testing of intelligent temperature transducer and implements a simple application of this transducer is shown in Fig. 13. The main components of this system are the intelligent sensor, the temperature probe, the programmable logic controller (PLC), the power supply and several auxiliary devices and circuits.

The temperature around the probe increases when a power resistor ( $R_p=39\Omega / 25W$ ) is supplied with 24Vdc, and a cooler ( $C_l$ ) is used to lower the temperature. A three-terminal positive regulator with a 12Vdc fixed output voltage supplies the cooler. The power resistor and the cooler are positioned near the Pt100 resistance temperature detector.

The supply of power resistor and cooler can be controlled with mini toggle switches ( $K_R$  – for power resistor, and  $K_C$  – for cooler) or with PLC as shown in Fig. 14. When  $K_R$  is *on* and  $K_C$  is *off*, only  $Q_{R1}$  transistor is *on*, the current starts flowing through the control coil of  $REL_1$  relay and its contact (NO) becomes closed. This way, only the power resistor is supplied and the measured temperature rises. When  $K_C$  is *on* and  $K_R$  is *off*, only  $Q_{R2}$  transistor is *on*, the  $C_l$  cooler is connected to the DC supply (+12Vdc), and the Pt100 probe temperature decreases.

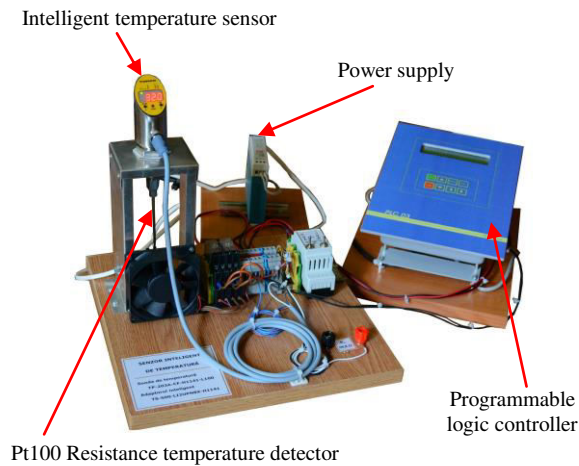


Fig. 13 . Experimental system for studying the intelligent temperature transducer.

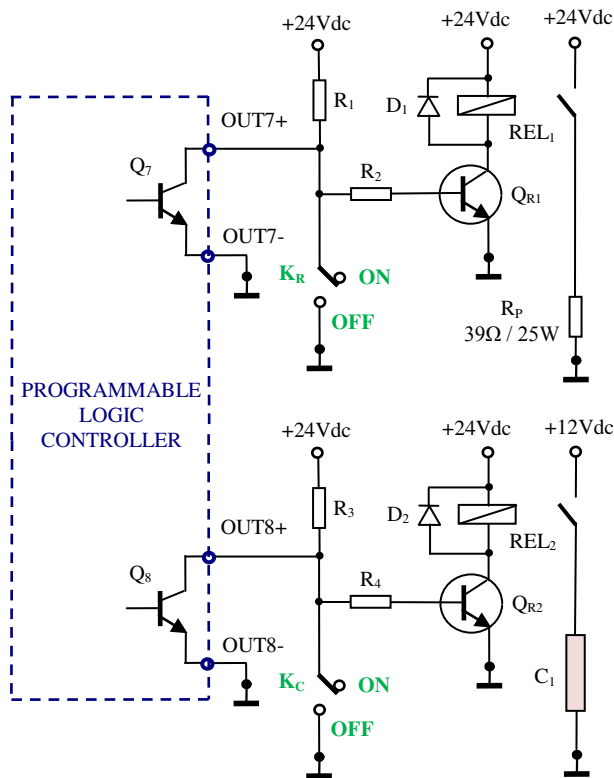


Fig. 14. The voltage supply control for power resistor and cooler.

The undergraduates supply the laboratory model excepting PLC. Initially,  $K_R$  and  $K_C$  mini toggle switches will be *off*. The testing of intelligent temperature transducer consists in

studying all three operating modes (*Run*, *Menu*, and *Programming*),

locking/unlocking the access to *Mode*, *Set* and *Enter* buttons for secure programming,

testing the operation of both switching functions and analogue output.

The explanations and graphical representations presented above in this paper and the information from (Catalog, 2014) and (User manual, 2012, 2016) are very important for the transducer's testing. The students set the desired values/types for the characteristic points, output functions, analogue ranges and more special functions using the clear menu structure presented in (Purcaru, 2017a).

The parameter settings for testing the temperature transducer functioning with two switching outputs are shown in Table 1. The undergraduates act  $K_R$  and  $K_C$  mini toggle switches for changing the measured temperature and then observe the intelligent sensor signalling (*Out 1* and *Out 2* LEDs, shown in Fig. 15a) during the temperature increasing and decreasing in accordance with the settings made.

Table 1. The parameter setting for two switching outputs

Parameter	Uni	ou1	SP1	rP1
Value	°C	Hno	35.0	32.0
Parameter	ou2	SP2	rP2	diS
Value	Fnc	37.0	30.0	50

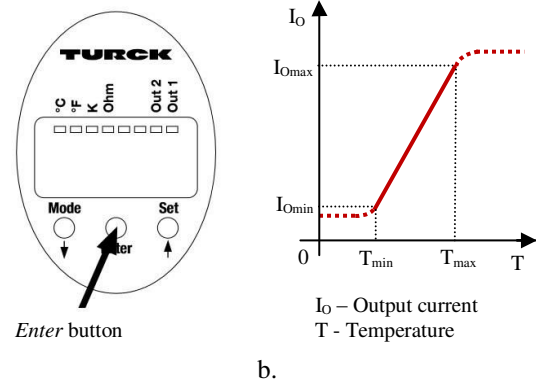


Fig. 15. a) Intelligent sensor signalling and buttons. b) Static transfer characteristic for analogue output.

The circuit from Fig. 16 allows testing the temperature transducer functioning with one analogue output.

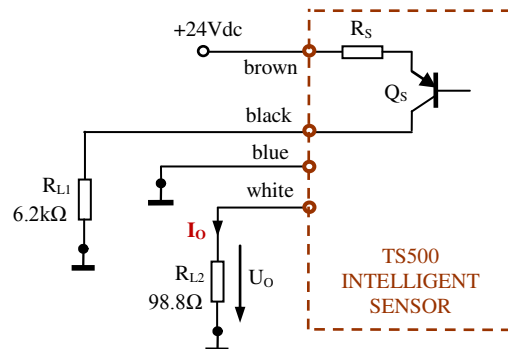


Fig. 16. Circuit for testing the temperature transducer functioning with one analogue output.

The undergraduates must change the settings for the second output as follows:  $ou2=4-20\text{mA}$ ,  $ASP=35.0$  and  $AEP=50.0$ . As a result, the measuring range is  $[T_{min}, T_{max}]=[35^{\circ}\text{C}, 50^{\circ}\text{C}]$ , and the corresponding output current range is  $[I_{Omin}, I_{Omax}]=[4\text{mA}, 20\text{mA}]$ . The undergraduates change the measured temperature (by using  $K_R$  and  $K_C$  mini toggle switches), measure the corresponding  $U_O$  voltage drop across the  $R_{L2}$  resistor (Fig. 16) and calculate the  $I_O$  output current through  $R_{L2}$ . Some of the measured and calculated values are given in Table 2 and they allow the drawing of the static transfer characteristic ( $I_O$  output current versus  $T$  temperature) shown in Fig. 15b. The students can observe the linearity of input-output dependence within the measuring range. Knowing  $I_O$  output current, the measured  $T$  temperature can be calculated:

$$T = \frac{\Delta I_O \cdot T_{min} - \Delta T \cdot I_{Omin}}{\Delta I_O} + \frac{\Delta T}{\Delta I_O} I_O \quad (1)$$

We denote  $\Delta T=T_{max}-T_{min}$ , and  $\Delta I_O=I_{Omax}-I_{Omin}$ .

Table 2. Experimental results for the analogue output

$T[^{\circ}\text{C}]$	30.0	32.0	33.0	35.0
$U_O[\text{V}]$	0.341	0.341	0.341	0.395
$I_O[\text{mA}]$	3.451	3.451	3.542	3.998
$T[^{\circ}\text{C}]$	38.0	41.0	44.0	47.0
$U_O[\text{V}]$	0.711	1.027	1.344	1.659
$I_O[\text{mA}]$	7.196	10.395	13.603	16.791
$T[^{\circ}\text{C}]$	50.0	52.0	53.0	55.0
$U_O[\text{V}]$	1.976	2.2	2.26	2.26
$I_O[\text{mA}]$	20.000	22.267	22.87	22.87

If the temperature exceeds by more than 5% the measuring range, *OL* for overload, respectively *UL* for underload is displayed.

An on-off temperature control system is implemented using the programmable logic controller; PLC monitors the sensor's switching output 1 and controls the voltage supply of the  $R_P$  power resistor and  $C_I$  cooler. The settings for output 1 are those specified in Table 1. The intelligent sensor connection to input 8 of PLC is performed as shown in Fig. 12, and the supply control of power resistor and cooler is presented in Fig. 14. A program which allows keeping the temperature between  $32^{\circ}\text{C}$  and  $35^{\circ}\text{C}$  is loaded onto PLC.

Firstly, the undergraduates must supply the PLC, intelligent sensor and auxiliary circuits, with the  $K_R$  and  $K_C$  mini toggle switches *off*. Then the program starts and students observe the temperature control. When  $Q7$  output transistor of PLC is *off*,  $Q_{R1}$  transistor is *on* and the current starts flowing through the control coil of REL1 relay; its *NO* contact becomes closed, the power  $R_P$  resistor is connected to the DC supply (+24Vdc) and the temperature increases near the Pt100 probe. If  $Q7$  transistor is *on*,  $Q_{R1}$  is *off*, the current stops flowing through the coil and the temperature decreases. The cooler supply is controlled in the same way using the  $Q8$

output transistor of PLC,  $Q_{R2}$  external transistor and  $REL_2$ .

### 3.3 Experimental System for Testing Ultrasonic Sensors

An experimental system allows undergraduates to test the operating and programming of the above presented ultrasonic sensors. The system is shown in Fig. 17 with RU30 and QS18 sensors mounted on a support plate, the PLC programmable logic controller and the power supply for sensors. The projection of each sound cone is figured on the support plate and a ruler marking allows users to measure the distance to target.

The students supply QS18UPA ultrasonic sensor and then test the local programming (via push button) and observe the sensor signalling for both *Teach* method,

measure the blind zone, sensing range and detection zone for various objects (metal or non-metal, clear or opaque with different shapes and sizes).

The undergraduates must connect the sensor to the programmable logic controller, as shown in Fig. 18, for testing the remote programming of QS18UPA sensor. Three programs (denoted *1 Pulse*, *3 Pulse*, and *4 Pulse*) are loaded on the PLC to generate three commands for the sensor (User manual, 2007).

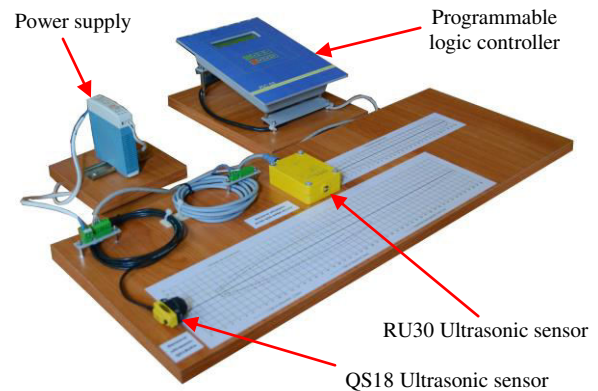


Fig. 17. Experimental system for testing ultrasonic sensors.

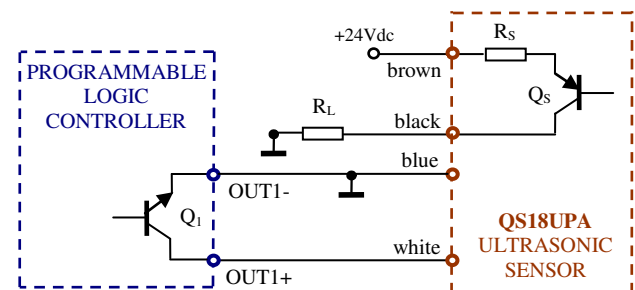


Fig. 18. The QS18UPA ultrasonic sensor connection to the programmable logic controller for remote programming.

*1 Pulse* program allows implementing of both *Teach* methods for sensor programming as via push button. If *3 Pulse* program is selected, three pulses are sent to the remote line of sensor to toggle between *NO* and *NC*

operation. The *4 Pulse* program is selected for locking/unlocking the access to push button.

The students supply RU30 ultrasonic sensor and then move the same various objects relatively to the sensible face and observe the sensor signalling, measure the detection zone for different targets, test the local programming by adjusting the upper switching limit via potentiometer.

### 3.4 Experimental System for Testing Inductive and Capacitive Proximity Sensors and Implementing a Motion Control System

A light metallic object can move inside a tunnel and one proximity sensor (inductive/capacitive) is mounted on a cooler at each tunnel's extremity. The inductive and capacitive proximity sensors will be used to detect the limit positions for the metallic object. These components together with other auxiliary elements are mounted on a support plate. The experimental system for studying proximity sensors (shown in Fig. 19) also contains a programmable logic controller (PLC) and a power supply.

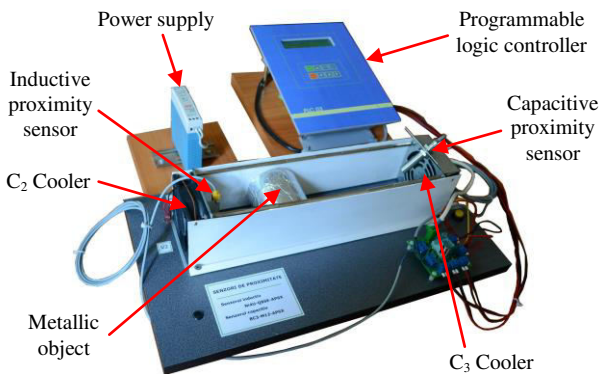


Fig. 19. Experimental system for testing inductive and capacitive proximity sensors and implement a motion control.

Both proximity sensors are powered simultaneously by 24Vdc supply. Each sensor testing involves checking its operation for more objects from different materials and with various shapes and sizes. The undergraduates observe the sensor signaling and influence of the object shape, size, material and orientation on the sensor sensitivity (the inductive sensor can detect only metallic objects). The students observe and measure each detection zone and hysteresis; the detection zone of capacitive sensor is adjusted via potentiometer.

A motion control system is implemented with the components of this experimental system: the light metallic object permanently moves from one extremity to the other of the tunnel. The program loaded on the PLC allows the monitoring of the switching outputs of both proximity sensors and controlling the voltage supply of two coolers.

The sensor connection to PLC is shown in Fig. 12 and explained above; the inductive sensor output is connected to input 5 of PLC, and the capacitive sensor output is connected to input 6. Each proximity sensor activates when the object reaches that tunnel extremity.

The power supply control of  $C_2$  and  $C_3$  coolers using the output 5 of PLC is shown in Fig. 20. The operation of the relay control circuit was presented above (Fig. 14). One of the coolers is powered at one time and pushes the metallic object to the other extremity of the tunnel.

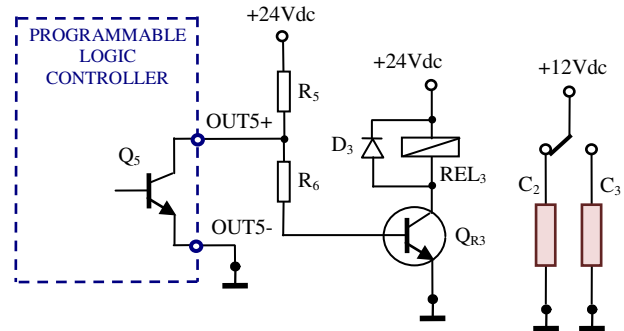


Fig. 20 . The power supply control of coolers using programmable logic controller.

When the inductive sensor detects the metallic object, the  $Q_5$  transistor becomes *off*,  $C_2$  cooler is powered by 12Vdc and it moves the object toward the capacitive sensor. If the capacitive sensor is activated,  $Q_5$  transistor is *on*,  $C_3$  cooler is powered and the metallic object moves toward the inductive sensor.

## 4. CONCLUSIONS

This paper presents a guideline and three experimental systems for studying several sensors and implementing simple applications of these devices. The users thoroughly understand the sensors' operation and programming also acquiring practical skills using inductive, capacitive and ultrasonic sensors, resistance temperature detector, intelligent temperature sensor and programmable logic controller. The engineering undergraduates learn to design and implement a temperature control system and a motion control system with the studied sensors.

## REFERENCES

- Busslinger, A., Lampe, K., Beuchat, M. and Lehmann B. (2001). A comparative in vitro study of a magnetostrictive and a piezoelectric ultrasonic scaling instrument, *Journal of Periodontal & Implant Science*, Issue 28(7), pp. 642-649.
- Frota, M. N. and Finkelstein, L. (2006). Education in metrology and instrumentation from the engineering perspective, *Journal of Engineering Education*, Vol. 25, Issue 1, pp. 49-65.
- Frota, M. N. and Finkelstein, L. (2013). Thoughts on the education in measurement and instrumentation: A review of requirements, *Measurement. Journal of the*

- International Measurement Confederation*, Vol. 46, pp. 2978–2982.
- Ibrahim, D. (2015). Development of a low-cost educational liquid-level sensor circuit, *International Journal of Electrical Engineering Education*, Vol. 52(2), pp. 168–181.
- Koch, F. D., Dirsch-Weigand, A., Awolin, M., Pinkelman, R. J. and Hampe, M. J. (2017). Motivating first-year university students by interdisciplinary study projects, *European Journal of Engineering Education*, Vol. 42, Issue 1, pp. 17-31.
- Olowokere, D. and Ajofoyinbo, A. (2015). A Framework for Integrating Intelligent Sensor Measurement Data into Engineering Education, *Proceedings of The 122nd Annual Conference of the American Society for Engineering Education*, Paper ID – 11966, Seattle, USA.
- Özerdem, Ö. C. (2016). Design of two experimental setups for programmable logic controller (PLC) laboratory, *International Journal of Electrical Engineering Education*, Vol. 53(4), pp. 331–340.
- Purcaru, D. M. (1998). Experimental sensory device used for touching an object, in *Proceedings (Vol. Devices and Sensors) of The 6<sup>th</sup> Biennial Conference on Electronics and Microsystems Technology*, pp. 59-62, Tallinn Technical University Press, Estonia.
- Purcaru, D.M., Purcaru, I. (2000). Experimental system for studying some displacement sensors, *Proceedings of The International Symposium on Systems Theory, Automation, Robotics, Computers, Informatics, Electronics and Instrumentation*, pp. E106-E109, Universitaria Press, Craiova, Romania.
- Purcaru, D., Gordan, C., Purcaru, I., Niculescu, M., Proca, V. and Vintila, A. (2009a). Bending stress measurement system and procedure for experimental training of undergraduated on electronics and measurement techniques, *WSEAS Transactions on Advances in Engineering Education*, Issue 5, Vol. 6, pp. 131-141.
- Purcaru, D., Niculescu, E. and Gordan, C. (2009b). Electronic measurement system and procedure for optical encoder and force sensor studying, *Journal of Electrical and Electronics Engineering*, Vol. 2, No. 2, pp.181–186, University of Oradea Press, Oradea, Romania.
- Purcaru, D., Gordan, C. and Purcaru, A. (2011). Application of the I-7000 remote controllable data acquisition modules in a measurement system with inductive sensors, *Journal of Electrical and Electronics Engineering*, Vol. 4, No. 1, pp. 203–206, University of Oradea Press, Oradea, Romania.
- Purcaru, D. (2012). *Instrumentation, sensors and measurement systems. Practical works (Instrumentatie, senzori si sisteme de masurare. Lucrari practice)*, Universitaria Press, Craiova, Romania, pp. 126-215.
- Purcaru, D., Purcaru, A. and Radulescu, V. (2017a). Temperature measurement and control system for engineering education, *Proceedings of The 18th International Carpathian Control Conference*, in press.
- Purcaru, D., Gordan, I. M. and Purcaru, A. (2017b). Study, testing and application of proximity sensors for experimental training on measurement systems, *Proceedings of The 18th International Carpathian Control Conference*, in press.
- Yousefimanesh, H., Robati, M., Kadkhodazadeh, M. and Molla, R. (2012). A comparison of magnetostrictive and piezoelectric ultrasonic scaling devices: an in vitro study, *Journal of Periodontal & Implant Science*, Issue 42(6), pp. 243–247.
- Catalog – Turck Instrumentation products. (2014).
- Catalog – Turck Proximity Sensors. (2011).
- Catalog – Uprox+ Inductive factor 1 sensors. (2012).
- Catalog – Turck Capacitive sensors. (2015).
- Catalog – Overview ultrasonic sensors. (2016).
- Catalog – Pepperl+Fucus Ultrasonic sensors. (2005)
- Datasheet – MDR-20 Power supply. (2007).
- Datasheet – QS18 Ultrasonic sensor. (2010).
- Datasheet – Turck Temperature probes. (2015).
- Datasheet – Ultrasonic sensor diffuse mode sensor RU30-Q30-AP8X-H1141. (2016)
- Datasheet – Inductive sensor Ni4U-Q8SE-AP6X-V1131. (2017a).
- Datasheet – Capacitive sensor BC3-M12-AP6X-H1141. (2017b).
- User manual – Turck Temperature sensor series TS-400/500. (2012, 2016).
- User manual – Turck Ultrasonic sensors. (2007, 2013).

# Pruning Methods and Splitting Criteria for Optimal Decision Trees Algorithms

Lavinu Aurelian Bădulescu

*Faculty of Automation, Computers and Electronics, University of Craiova, Craiova, Romania (e-mail: badulescu@automation.ucv.ro)*

---

**Abstract:** Decision Trees are some of the most well-liked Data Mining algorithms for prediction and classification. We will present in this paper the performance of the Decision Trees (DT) induced with 13 splitting criteria over Census Income database taken from UCI Knowledge Discovery in Database Archive. The research involved the growing of the DT on a training data set, the extraction of decision rules, the pruning of the DT using two pruning methods: error-based and pessimistic and lastly, the DT execution on the test data. A good selection of an attribute used to split the data set at each DT node will optimize the classification accuracy. The biggest values for the classification accuracy are systematically obtained by error-based pruned DT. In the same time, the best performances for classification error rate on the test data set, data absolutely not known at the training of DT, were obtained by the symmetric gini index splitting criterion. We conclude the paper with a discussion on related work.

**Keywords:** decision trees; classification error rate; splitting criterion; pruning method; decision rule.

---

## 1. INTRODUCTION

In classification and regression applications one of the most efficient non-parametric method is the Decision Trees (DT). DT are hierarchically organized data structures for supervised learning by which the input space is splitted into local areas in order to predict the dependent variable (Barros, 2015).

As is stipulated in (Shmueli, 2017), after induction and pruning phases, DT are computationally cheap to execute even on large records. The DT are highly automated, robust to extreme values, and able to handle lost values.

We will present in this paper the performance of the DT induced with 13 splitting criteria over *Census Income database* taken from UCI Knowledge Discovery in Database Archive (<http://kdd.ics.uci.edu/databases/census-income/census-income.html>). During this mining experiment, we construct DT in order to get some classification rules. We set an attribute named “class  $\leq 50K$ ,  $> 50K$ ” as class target attribute since we want to learn, based on census data, the suitable classification of income (income  $\leq \$50K/yr$  or income  $> \$50K/yr$ ) for each individual.

For the DT building, 13 splitting criteria have been tested. The research involving the growing of the DT on a training data set (actually, there were induced 13 distinct DT by means of 13 splitting criteria at the splitting of a DT node), the pruning of a DT (the 13 DT from the prior stage are pruned, by means of two pruning methods: error-based pruning and pessimistic pruning method (Rokach, 2015) and lastly, the DT execution on the test

data – different data of the ones used at the training of the DT - to compute the classification error rate of every DT.

Together with the value of the dimension of the file for every DT induced with a distinct splitting criterion, we have also noticed the values of the height and the number of nodes of every DT. The most important parameter for the performance of each DT, the classification error rate on the test data set, data absolutely not known at the building of DT, has been highlighted.

The rest of the paper is organized as follows. At the beginning we review the splitting criteria used in this paper and the *Census Income database* specifications. Then we will examine the behaviour of the splitting criteria on the growing, extraction of decision rules, pruning and execution of the DT over the *Census Income database*. Lastly, we finish the paper with a discussion on related work.

## 2. SPLITTING CRITERIA. DATA FEATURES

Splitting criteria used in this paper for induction of DT are: Bayesian-Dirichlet metric (*bd*), information gain (*ing*), stochastic complexity (*stc*), Gini index (*gini*), modified Gini index (*ginim*), symmetric Gini index (*ginis*),  $\chi^2$  (*hi2*), relevance (*rlv*), average absolute weight of evidence (*wevd*), information gain ratio (*ingr*), symmetric information gain ratio (*singr*), symmetric specificity gain ratio (*sigr*), RELIEF measure (*relief*). All of them are developed in (Bădulescu, 2007) with specification of publications where they are for the first time presented. For this reason we will not reiterate the theoretical presentation of these splitting criteria in this paper. In (Bădulescu, 2007) we presented the behavior of

the splitting criteria on the growing, pruning and execution of the DT over the three databases: *Abalone*, *Cylinder Bands* and *Image Segmentation* taken from UCI Machine Learning Repository. The results showed superiority of the error-based pruning method or confidence level pruning method. Good values for classification accuracy had obtained *stc* (*Abalone*) and *ingr* (*Cylinder Bands*) splitting criteria.

The experiments we wish to present in this paper will target *Census Income*, a much larger database with much more attributes and much more samples.

All experiments on *Census Income database* were conducted on a PC Intel i5-6400 CPU 2.70GHz with 4.00 GB RAM, running Windows 10 Pro and the code was written in C.

*Data features.* The data contain 40 attributes, continuous (7) and nominal (33) of occupational and demographical type, plus the class label (*income*). Total number of cases: 299,285. Number of training cases: 199,523, out of which duplicated or contradictory cases: 46,716. Number of testing cases: 99,762, out of which duplicated or contradictory cases: 20,936.

The prediction task is to determine the *income* for a person represented by a record in the dataset. The incomes were divided at the 50K\$ level in order to state a problem of binary classification.

### 3. EXPERIMENTAL RESULTS

#### 3.1 The DT induction with 13 different splitting criteria

There are two groups for the performances realized by the 13 splitting criteria for the induction of DT. The first group of 8 criteria (*ing*, *gini*, *hi2*, *rlv*, *ginis*, *ginim*, *relief*, *wevd*) realizes very good performances for the DT growth time and for the size of the file that contains the unpruned DT. Next group contains 5 criteria (*ssgr*, *bd*, *ingr*, *singr*, *stc*) with greater values for the two features presented.

At the extraction step of the decision rules from unpruned DT we noticed the decision rules number and the size of the file which contains these decision rules for each of the 13 criteria. The best values for the decision rules number are gained by a number of 12 criteria: *ingr*, *singr*, *bd*, *ginis*, *gini*, *hi2*, *ing*, *rlv*, *ginim*, *stc*, *relief*, *wevd*, for which also the size of the file containing these decision rules is relatively small. A single criterion (*spcgr*) realizes weaker performances though.

The differences between the numbers of decision rules, which the 13 criteria need for the construction of the classifier is very big. The maximum value of the decision rules number is 4 times bigger than the minimum value. The maximum number of decision rules is 24,549, the minimum number is 5,852 and the standard deviation is 4,352.28.

The best value for the classification error rate on the test data, for the unpruned DT, is obtained by *ginis* criterion

(5.82%), and the poorest performance is obtained by *ssgr* criterion (6.90%).

#### 3.2 Error-based pruning DT

The unpruned DT, for all 13 criteria, was pruned with error-based method. Excepting one criterion (*ingr*), which builds a very large pruned DT file: 3,962 KB, unlike the average of all 13 criteria: 617 KB, or the minimum value: 130 KB, all the other 12 criteria have approximately equal values for the DT file pruning time and for the pruned DT file size.

The differences between the numbers of decision rules, which the 13 criteria need for the construction of the classifier is big. The maximum value of the decision rules number is almost 3 times bigger than the minimum value. The maximum number of decision rules is 2,201, the minimum number is 762 and the standard deviation is 395.54.

Unlike the unpruned DT, which presents a maximum number of decision rules, namely 24,549 (11 times bigger), a minimum number of 5,852 (almost 8 times bigger) and a standard deviation of 4,352.28 (11 times bigger), we can say that the performance “decision rules number” has obvious improved. Also, as we will next see, it has improved through the error-based pruning the classifier accuracy.

For the error-based pruning DT, one can obtain the best value for the classification error rate: 4.65% (*ginis* criterion). The worst value (maximum) for the classification error rate (5.44%, obtained by *ssgr* criterion) is better than the best value of classification error rate for unpruned DT (5.82% obtained by *ginis* criterion). At unpruned DT the highest value of the classification error rate was 6.90% obtained by *ssgr* criterion. We also perceive a reduction for the classification error rate standard deviation with the error based pruning of DT, from 0.29 to 0.22.

#### 3.3 Pessimistic pruning DT

Through the pessimistic pruning DT it has been established a decrease of the DT file size. Thus, the maximum value of the file size decreases from 15,395 KB to 3,776 KB (4 times), the minimum value decreases from 1,771 KB to 829 KB (2 times) and the average value from 5,519.46 KB to 1,533 KB (3.6 times). The standard deviation decreases much more for the DT file size, from 4,901.44 to 735.50 (6.6 times).

The tree's height has, at unpruned DT, a maximum value of 1,033 levels which through the pessimistic pruning of DT decreases to 423 (2.4 times). The minimum value for unpruned DT is of 18 levels; we can notice that it is a bit modified through the pessimistic pruning of DT (17 levels). However, the average decreases from 254.15 levels to 60.62 levels (4.2 times). For this performance the standard deviation decreases from 378.20 to 109.63 (3.4 times).



The number of tree's nodes has at unpruned DT a maximum value of 42,141 nodes which through the pessimistic pruning of DT decreases to 9,691 (4.3 times).

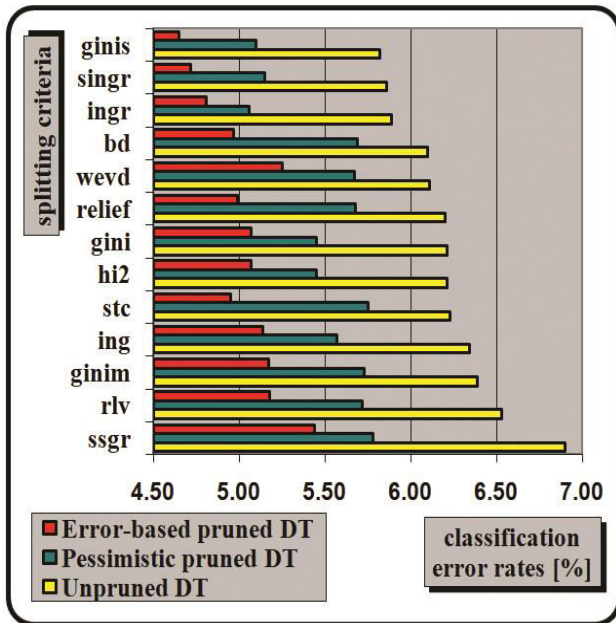


Fig. 1. Classification error rates for DT execution on test data, ordered by unpruned DT execution values.

The minimum value of unpruned DT is of 9,555 nodes; we can notice that it decreased through the pessimistic pruning of DT to a value of 5,894 nodes (1.6 times). However, the average decreases from 18,772.38 nodes to 7,483.15 nodes (2.5 times). For this performance, the standard deviation decreases from 7,738.82 to 940.11 (8.2 times).

The tree's height presents for error-based pruned DT a maximum value of 861 levels, for which the pessimistic pruned DT is of 423 levels (two times smaller). The minimum value for error-based pruned DT is of 13 levels; at the pessimistic pruned DT this value is slightly smaller: 17 levels. The average decreases from 91 levels (error-based pruning) to 60.62 levels (pessimistic pruning). For this performance the standard deviation decreases from 231.97 (error-based pruning) to 109.63 (pessimistic pruning).

The nodes number of the tree presents for error-based pruned DT a maximum value of 3,641 nodes which at the pessimistic pruning DT is of 9,691 (almost 3 times higher). The minimum value for error-based pruned DT is of 1,377 nodes, but for pessimistic pruning the minimum value of the number of nodes is of 5,894 nodes (almost 4 times higher). The average also increases from 2,128.77 nodes to 7,483.15 nodes (3.5 times). For this performance the standard deviation increases from 576.00 to 940.11.

Conclusively, we may say that for the *Census Income database*, the pessimistic pruning method builds less deeper DT, but with more nodes than the error-based pruning method.

The differences between the decision rules number which require the 13 criteria needed to construct the classifier

are relatively small. The maximum value of decision rules number (5,639) is about 1.5 times larger than the minimal value (3,507). The standard deviation is 558.08.

Towards to the unpruned DT, presenting a maximal decision rules number of 24,549 (4.4 times greater), a minimum number of 5,852 (1.7 times greater) and a standard deviation of 4,352.28 (7.8 times greater), we can say that the performance of the decision rules number has increased significantly with the pessimistic pruning of DT. As we are about to see, the accuracy of the classifier it has also improved through the pessimistic pruning.

Towards to the error-based DT, which presented a maximum decision rules number of 2,210 (2.6 times less), a minimum number of 762 (4.6 times less) and a standard deviation of 395.54 (1.4 times less), we can say that the performance of the decision rules number is better for the error-based pruned DT towards the pessimistic pruned DT. We will notice that we can say the same thing about the most important performance of the classifier: the classification accuracy on the test data. It is proved that the best performance at the pessimistic pruned DT execution on test data is realized by the *ingr* criterion (5.06%). But even the less good performance, realized by the *ssgr* criterion (5.78%), is just a little bit higher.

### 3.4 Summarized table with decision rules number and classification error rate for the three types of DT

From the values of Table 1 and from the associated chart (see Fig. 1) we can see that the best performance for the classification error rate on the *Census Income database*, is obtained by error-based pruned DT through *gini* criterion (4.65%). This criterion, also for the same error-based pruned DT, obtains even the smallest decision rules number (4,634). The weakest performance for the classification error rate on the *Census Income database*, is obtained by unpruned DT through *ssgr* criterion (6.90%). This criterion, also for the same unpruned DT, obtains even the highest decision rules number (6,888). Let's notice that the *gini* criterion which, for the unpruned DT obtains the best performance for the classification error rate (5.82%) and the smallest decision rules number (5,809), when pruning the DT with the error-based pruning method improve the performance, and, for the pessimistic pruned DT, it deteriorates the performance.

The smallest values for the classification error rate are systematically obtained by error-based pruned DT, the average of the classification error rate for the 13 splitting criteria is 5.03%. On the second place, with average values for the classification error rate, stands pessimistic pruned DT; the average of the classification error rate for all 13 splitting criteria is 5.52%.

The biggest values for the classification error rate on *Census Income database* are made by unpruned DT; the average error classification rate for all 13 splitting criteria is 6.21%. The standard deviation, representing the dispersal of the values of the classification error rate, is 0.22 for error-based pruning method and 0.26 for pessimistic pruning method, whereas, standard deviation

for the unpruned DT classification error rate is the highest (0.29).

Considering the values achieved for the classification error rate at the three category of DT, we can conclude that throughout the pruning of DT, the accuracy of the classification improves and the spreading of the values of the classification error rate diminishes (the standard deviation decreases).

Table 2. Summarized table with decision rules number and classification error rate for all types of DT

No	Criterion	Unpruned DT		Error-based pruned DT		Pessimistic pruned DT	
		Rules #	Classification error rate [%]	Rules #	Classification error rate [%]	Rules #	Classification error rate [%]
1	bd	6078	6.09	4959	4.97	5676	5.69
2	ing	6323	6.34	5131	5.14	5553	5.57
3	stc	6211	6.23	4935	4.95	5732	5.75
4	gini	6192	6.21	5060	5.07	5435	5.45
5	ginim	6370	6.39	5155	5.17	5713	5.73
6	ginis	5809	5.82	4634	4.65	5091	5.10
7	hi2	6195	6.21	5061	5.07	5440	5.45
8	rlv	6513	6.53	5170	5.18	5711	5.72
9	wevd	6100	6.11	5240	5.25	5656	5.67
10	ingr	5877	5.89	4794	4.81	5051	5.06
11	singr	5855	5.87	4708	4.72	5143	5.16
12	ssgr	6888	6.90	5432	5.44	5767	5.78
13	relief	6182	6.20	4978	4.99	5667	5.68
	average	6199.54	6.21	5019.77	5.03	5510	5.52
	maximum	6888	6.90	5432	5.44	5767	5.78
	minimum	5809	5.82	4634	4.65	5051	5.06
	standard deviation	291.34	0.29	220.72	0.22	259.57	0.26

#### 4. CONCLUSION AND FUTURE WORK

On the link (<http://kdd.ics.uci.edu/databases/census-income/census-income.names>) where *Census Income database* is presented, there are some values for the classification error rate obtained by different algorithms: 4.6% (C5.0 boosting), 4.7% (C5.0), 4.7% (C5.0 rules), 4.8% (C4.5), and 23.2% (Naïve-Bayes). Please note that the value (4.65%) for classification error rate on DT induced with *ginis* splitting criterion and pruned with error-based method, equals with the best value obtained by the other algorithms, taking into account only the first digit after the dot.

In (Holmes et al., 2004) the original values of the training cases number and of the test cases number have been augmented to 249.285 and, respectively decreased to 50.000. It is clear that increase of the training cases number, followed by a minimization of the test cases number, can only lead to the decrease of the classification

error rate values. Thus are accomplished the following classification error rates: 4.46% (ADTree), 4.62% (OTC), 4.69% (C4.5), 4.72% (BC4.5), 5.44% (C4.5C), “out of memory” (BC4.5C). The best value, achieved through the method previously explained, is 4.46%, slightly smaller than our best value: 4.65%, gained on the original values of the training and test cases number.

In (Oza et al., 2001) the original values for the number of training samples vs. the number of testing samples are being kept, but the value acquired for the classification accuracy on the test data is being provided only graphically. Exploring the diagram we can certainly say that this value is fewer than 95%, it is around 94%. So this means a classification error rate greater than 5%, maybe even 6%. This value is lower than the best value for the classification error rate achieved by us, namely 4.65%.

In (Caragea, 2004) the execution of the Naïve Bayes algorithm (Weka implementation) on *Census Income database* ends with “out of memory” error, whereas the implementation of AirDM with INDUS produces an error rate of 23.7826%.

In (Frank et al., 2002) the original values of the training cases number and of the test cases number have been adjusted to 224.285 and, respectively to 50.000; 25.000 cases have been used for validation. With the adjusted values for the distribution of cases number, it is achieved a classification error rate of 4.43% (LogitBoost), slightly smaller value than our best value: 4.65%, obtained on the original values of the training and test cases number.

The experiments made with XMiner in (Calders et al., 2007) don't supply any value for the classification error rate. In (Bay, 2001) the classification error rate isn't mentioned as well, whereas it is affirmed that the execution under the Apriori algorithm has finalized with the error „out of memory”. There are many others researches on *Census Income database* using different Data Mining techniques from rough sets in (Wang et al., 2009) to clustering in (Show-Jane et al., 2009).

To conclude, the best performances obtained by the splitting criteria used in our experiments on *Census Income database*, is of 4.65% (classification error rate on the test data set) and 4.634 (number of decision rules), both obtained by the *ginis* splitting criterion and error-based pruning method. The DT pruned with error-based pruning method achieves the best values for average, maximum, minimum, and standard deviation vs. DT pruned with pessimistic pruning method or unpruned DT.

We must to mention a limitation of our results: in evaluation by classification accuracy we have assumed equal error costs, but in the real world this is not always true. Further work must to take into account this limitation. The experiments we wish to perform next will target much larger databases with many attributes and many samples on which we want to verify the performances of much more splitting criteria and much more pruning methods.

## ACKNOWLEDGMENT

We want to note the assistance we received from Hettich, S. and Bay, S. D., Irvine, CA: University of California, Department of Information and Computer Science.

## REFERENCES

- Bădulescu, L.A. (2007). Attribute selection measure in decision tree growing. In Nicolae, I.D., and Doicaru, E. (eds.), *Proc. of the International Symposium on Systems Theory, Automation, Robotics, Computers, Informatics, Electronics and Instrumentation - SINTES 13*, vol. 2, pp. 1-6, Ed. Universitaria, Craiova.
- Barros, R.C., de Carvalho, A.C.P.L.F., and Freitas, A.A. (2015). *Automatic design of decision-tree induction algorithms*, p. 8, Springer International Publishing, Cham Heidelberg New York Dordrecht London.
- Bay, S. D. (2001). Multivariate discretization for set mining, In Wu, X. (ed.), *Knowledge and information systems*, vol. 3, issue 4, pp. 491–512, Springer-Verlag, New York.
- Calders, T., Goethals, B., and Mampaey, M. (2007). Mining itemsets in the presence of missing values, In Cho, Y., Wainwright, R.L., Haddad, H., Shin, S.Y., and Koo, Y.W. (eds.), *Proc. of the 22<sup>nd</sup> Annual ACM Symposium on Applied Computing*, ACM Press, New York.
- Caragea, D. (2004). *Learning classifiers from distributed, semantically heterogeneous, autonomous data sources*, PhD thesis, pp. 162-163, Iowa State University.
- Frank, E., Holmes, G., Kirkby, R., and Hall, M. (2002). Racing committees for large datasets, In Lange, S., Satoh, K., and Smith, C.H. (eds.), *Lecture Notes In Computer Science, Proc. of the 5<sup>th</sup> International Conference on Discovery Science*, vol. 2534, pp.153–164, Springer-Verlag, London.
- Holmes, G., Kirkby, R., and Pfahringer, B. (2004). Mining data streams using option trees, In Aguilar-Ruiz, J., and Gama, J. (eds.), *Proc. of the 1<sup>st</sup> International Workshop on Knowledge Discovery in Data Streams, held in conjunction with the 15<sup>th</sup> European Conference on Machine Learning and the 8<sup>th</sup> European Conference on the Principles and Practice of Knowledge Discovery in Databases*, pp. 75-84, Pisa, Italy.
- Oza, N.C., and Russell, S. (2001). Experimental comparisons of online and batch versions of bagging and boosting, In Provost, F., and Srikant, R. (eds.), *Proc. of the 7<sup>th</sup> ACM SIGKDD International Conference on Knowledge Discovery and Data Mining*, pp. 359–364, Morgan Kaufmann, San Francisco, California.
- Rokach, L., Maimon, O. (2015). *Data mining with decision trees. Theory and applications*, 2<sup>nd</sup> ed., pp. 71-72, World Scientific Publishing Co. Pte. Ltd., Singapore.
- Shmueli, G., Bruce, P.C., Stephens, M.L., Patel, N.R. (2017). *Data mining for business analytics. Concepts, techniques, and applications with JMP Pro*, p. 183, John Wiley & Sons, Hoboken, New Jersey, USA.
- Show-Jane, Y., and Yue-Shi, L. (2009). Cluster-based under-sampling approaches for imbalanced data distributions, In Lin, B. (ed.), *Expert Systems with Applications: An International Journal*, vol. 36, issue 3, pp. 5718-5727, Pergamon Press Ltd., United Kingdom.
- Wang, S., and Wang, H. (2009). Optimal use of incomplete data in rough sets applications, In Hojati M. (ed.), *Proc. of the 30<sup>th</sup> Annual Conference of the Administrative Sciences Association of Canada: Management Science Division*, vol. 30, no. 2, pp.8:1-11, ASAC, Niagara Falls, Ontario, Canada.

# Diagnosis Melanoma Skin Cancer Using ABCD Rule, Statistic Texture Feature and Lesion Symptoms

Faiq Baji\*, Mihai Mocanu\*\*

*Computer Science and Information Technology Department, Automation,  
Computers and Electronics Faculty, Craiova University, Craiova, Romania,*

*\*e-mail: faiq.baji2015@gmail.com*

*\*\*e-mail: mmocanu@software.ucv.ro*

---

**Abstract:** In recent years, there has been an obvious increase in the number of melanoma skin cancer patients. The diagnosis of skin cancer at an early stage is very important for effective treatment, but it is a challenging task in melanoma diagnosis. The irregularity of the lesion border is an important tools, it is used to reporting the melanoma during growth and propagation. In this paper, a new method is proposed to calculate Boundary Irregularity; this method is based on dividing the lesion according to the major axis into two sections, within each section, the Euclidean distance between the centre of the lesion and all pixel's borders is computed. The proposed method is based on the ABCD rule of dermatoscopy, statistical texture analysis, and lesion symptoms for melanoma skin cancer diagnosis. The computation of ABCD rule and texture analysis methods are based on the connected components objects for image segmentation. Several approaches have been introduced to identify the geometric shape features such as compactness, dispersion, and border irregularities. In this paper, the Stolz algorithm has been used for the diagnosis by calculating the Total Dermatoscopy Value (TDV) score. As it can be seen from the experimental results, the Boundary Irregularity method with the proposed method shows acceptable performance rates, the accuracy of the system is 90%

**Keywords:** Melanoma, Skin Cancer, Connected Components Objects, ABCD Rule, Texture Feature

---

## 1. INTRODUCTION

Skin cancer is a major public health problem. They are caused by the development of abnormal cells that have the potential to spread quickly to all organs/parts of the human body through the lymphatic system or blood (Nilkamal and Shweta, 2013). The skin cancer can classified into three main types: basal-cell skin cancer, squamous-cell skin cancer and melanoma. The first two types are less of common skin cancers, are known as non-melanoma skin cancer. Melanomas are the most aggressive yet harmless kind of skin cancer. Some Melanomas stay exactly the same and never change, but others can grow or change shape or color, have irregular edges, have more than one color, are itchy or bleeds (Ihab, 2016). The detection of malignant melanoma at its early stages considerably reduces morbidity and mortality, otherwise it can penetrate through the skin and disperse to the other parts of the body (Gopinathan and Nancy, 2016).

The computer aided diagnostics (CAD) supports the increase of the diagnosis accuracy as well as its speed. Computer is not more brilliant than human, but it may be able to obtain some information, like color variation,

asymmetry, border irregularities ratio, and texture features, that may not be easily perceived by the human eyes (Gopinathan and Nancy, 2016).

This paper proposes two Stages of the process of melanoma skin cancer diagnosis; the first stage uses the automatic method to diagnosis skin lesions. This approach evolves in three sequential steps. First, the lesion image is preprocessing using low-pass filters, linear contrast adjustment, and histogram equalization. Second, the lesion is segmented using connected components objects method. Third, the ABCD rule (Asymmetry, Border, Color, and Diameter) and texture features are extracted from the lesion. The ABCD rule is used to calculate the TDV score, whereas the texture analysis uses methods such as co-occurrence matrices calculus, and evaluation of texture features (such as energy, entropy, contrast and correlation during image processing).

The second stage represents the important information that can be obtained from the patient, it consists of information about the history of melanoma and palpation examinations which are discussed in subsection 5.4.1 and 5.4.2 respectively. All the processes of melanoma skin cancer diagnosis are shown in Fig. 1.

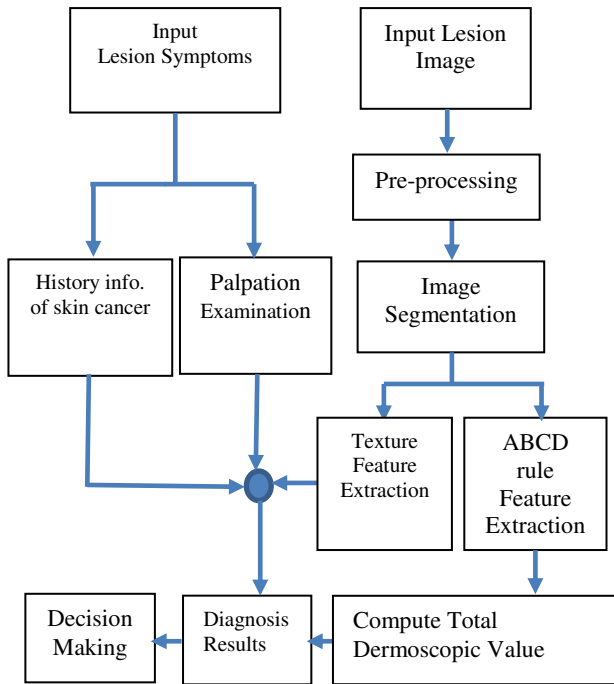


Fig. 1. Block diagram of proposed system.

## 2. Related Works

Various diagnosis systems for melanoma detection have been proposed, such as (Gopinathan and Nancy, 2016), (Sanjay et al., 2014), and (Bilqis et al., 2010), these works are using the Otsu threshold method and boundary tracing algorithm for image segmentation the lesion from the entire image. After extracting the features from the lesion, stolz algorithm has been used for the diagnosis through the calculation the (TDV) score. (Santiago and David, 2016) used the Asymmetry and Border features, which are considered to be the two main characteristics to accurately diagnose skin cancer, evaluates the differences between the digital regions border as well as the reference figure outline. This work uses as a square reference shape instead of the circle usually used in the continuous case. (Rashi and Saranjeet, 2015), discussed the affected skin texture profile correlation with malignant melanoma skin cancer and support vector machine (SVM) to classify the different skin images based on Gray Level Co-occurrence Matrix (GLCM) features. (Radu et al., 2010) described a method of an algorithm is using for automatic diagnosis to the malignancy of skin lesion which is based on two methods are local fractal dimension features and texture features that used GLCM to derived many statistics matrices (such as contrast, energy, and homogeneity). (Florence et al., 2011) proposed an image-based diagnosis method where images of skin disorder were used to classify skin diseases into broad category of either viral infected or bacterial infected.

## 3. PREPROCESSING

All skin images are inherently noisy due to errors associated with image acquisition. So, it is necessary to smooth out the segmented images before performing any

statistical analysis to boost statistical power (Kaveri and Chakravarthy, 2016).

Image preprocessing is an important step in image diagnosis. It is used to correct defects illumination, eliminating noise and small spots, and enhance the contours and contrast as much as possible without degrading the lesion. The Preprocessing proposed in this work consists of three steps: histogram equalization, linear contrast enhancements, and Gaussian filter (Nadia and Souhir, 2013). Histogram equalization and linear contrast manipulation are frequently used techniques to improving the degraded image contrast. When histogram equalization is approached, the mean brightness of the processed image is always the middle gray level with no regard to the input mean (Ravindra and Manish, 2015). Contrast enhancements, which improve the perceptibility of objects, are created by the difference in luminance reflected from two adjacent surfaces. In other words, contrast is the difference in visual properties that makes an object distinguishable from other objects and their background. Contrast enhancements are typically performed as a contrast stretch, is a linear transform that represented by maps the lowest values of a gray level  $GL_{min}$  in the image to zero and the highest value  $GL_{max}$  in the image to 255, with all other gray levels remapped linearly between zero and 255, as shown in the Fig. 2. This linear transform is given by (Geoff, 2009):

$$g'(x, y) = INT \left\{ \frac{255}{GL_{max} - GL_{min}} [g(x, y) - GL_{min}] \right\} \quad (1)$$

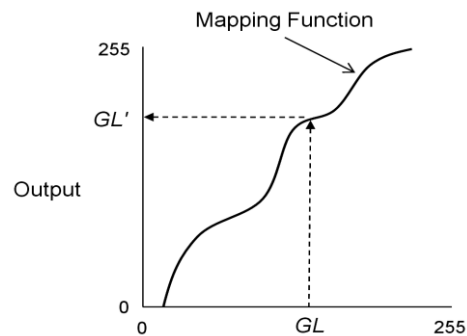


Fig. 2: A gray-level transform maps the gray levels to new values

Gaussian filters are a linear smoothing and low pass filters. The Gaussian smoothing filter is a fine filter to use for blur images and remove redundant feature and noise in two dimensions; the Gaussian function is:

$$G(x, y) = \frac{1}{2\pi\sigma^2} e^{-\frac{x^2 + y^2}{2\sigma^2}} \quad (2)$$

Where  $\sigma$  is the standard deviation of the distribution.

#### 4. IMAGE SEGMENTATION

Image segmentation involves image partitioning into multiple segments or regions of interest (ROI). It is a process of extracting and representing information from the image to group pixels together with the regions of similarity. The accurate separation of a skin lesion from the remaining surrounding skin plays an important role in the effectiveness of any image automated diagnosis system. To actually produce a segmentation of the image we need to group together all pixels with the same class that are adjacent to each other. Each set of pixels representing a segment is often referred to as a connected component (Nilkamal and Shweta, 2013).

##### 4.1 Connected Component

In image processing, a connected components algorithm detects regions of connected pixels, that have the same value by scanning an image, pixel-by-pixel (from top to bottom and left to right) in order to identify connected pixel regions, *i.e.* regions of adjacent pixels, which share the same set of intensity values  $V$ . (For a binary image  $V=\{1\}$ ; For instance, the binary image shown in Fig. 3-a, has three connected components).

Connected Components Labeling scans the segmented, binary image and groups its pixels into components based on pixel connectivity and marking each of them with a distinctive label, creating a Label Matrix, as shown in Fig. 3-b (Gleb, 2009).

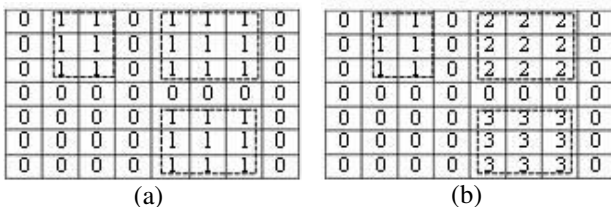


Fig. 3. (a) Image with 3-connected Components. (b) Labeled Connected Components

##### 4.2 Extraction of Connected Components

The extraction of connected components or objects from a binary image is important for many automated image analysis applications. Let  $A$  be a set that contains one or more connected components. We form an array  $X_0$  (of the same size as the array containing  $A$ ), whose elements are zeros (background), except the points of connected component in  $A$ , which correspond to one (foreground). The objective is to start with  $X_0$  and find all the connected components by the following iterative procedure (Gleb, 2009):

$$X_k = (X_{k-1} \oplus B) \cap A \quad k = 1, 2, 3, \dots \quad (3)$$

Where  $B$  is a suitable structuring element. The procedure terminates when  $X_k = X_{k-1}$  with  $X_k$  containing all the connected components of  $A$ , see Fig. 4.

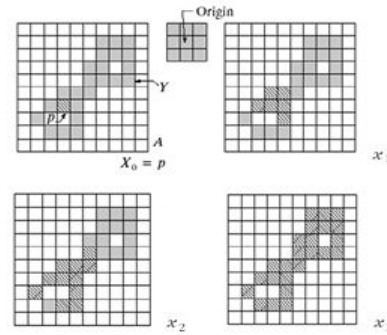


Fig. 4. Extraction of connected components.

#### 5. EXTRACT FEATURE

##### 5.1 Extract ABCD rule Feature

In automated diagnosis of skin lesions, feature extraction is based on the so-called ABCD-rule of dermatoscopy. These rules are represents by: asymmetry, border irregularity, color variance and diameter of the lesion and defines the basis for a diagnosis by a dermatologist (Sahil et al., 2016). Depending on the specification of ABCD rule, each extracted feature plays a distinctive role with its associative weight to calculate the TDV (Ihab, 2016).

##### 5.1.1 Asymmetry

An important feature used for realization the symmetry of the object shape, which is very useful in pattern analysis. If the normal mole area is divided into two sides according to the major axis and the minor axis, the edges of each side would match the other perfectly. In an asymmetrical mole, the two sides don't match in size or shape, as shown in Fig. 5. This is because the cells on one side of the mole are growing faster than the cells on the other side. Cancer cells tend to grow quicker than normal cells, and in irregular pattern. The mathematical formula used to determine the asymmetry value is given by the below relation:

$$Asymmetry = \left( \frac{\Delta p}{p} \right) \times 10 \quad (4)$$

Where,  $\Delta p$  is a Pixel difference,  $p$  is a total pixel count of a lesion. To estimate the asymmetry score, the melanocytic lesion is bisected by two  $90^\circ$  axes, if the shapes of both axes dermocosmically show asymmetric contours to shape, the asymmetry score is 2. If there is asymmetry on one axis only, the score is 1, if asymmetry is absent for both axes, the score is 0 (Gopinathan and Nancy, 2016). In the example of Fig. 5, the score of asymmetry is 2.

##### 5.1.2 Border Irregularity

The contour (border) of a skin lesion is the most significant factor in the early diagnosis of melanoma skin cancer (Santiago and David, 2016). In order to calculate border irregularity, there are several measures such as: compactness index, dispersion Irregularity, and different boundary

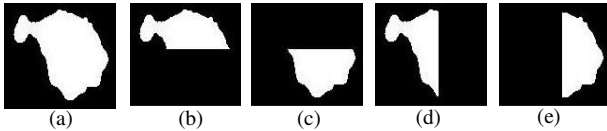


Fig.5. (a) shows the result of preprocess and segmented respectively, and (b, c, d, and e) show the divisions of the lesion according to the major axis and the minor axis respectively.

#### Compactness Index

Compactness index is one of the most common methods used for measuring and quantifying the circularity of the skin lesion. It is based on two parameters: the perimeter and area. The compactness measures the ratio between the area of the shape  $A_s$  and the area of a circle  $A_c$  can be traced with the same perimeter.

$$C = A_s/A_c = (\text{Area of a shape})/(\text{Area of circle})$$

$$A_c = \frac{P^2}{4\pi} \quad \text{Thus} \quad C(S) = \frac{4\pi A_s}{P^2} \quad (5)$$

Where  $A_s$  is the number of pixels of the lesion, and  $P$  (Perimeter) represents the number of edge pixels, compactness measures the efficiency with which a boundary encloses an area. For a circular region, the value of  $C(S) \simeq 1$ , which represents the maximum compactness value (Mark and Alberto, 2002).

#### Dispersion Irregularity(IR)

Dispersion IR (irregularity) is another feature suggested by (Mark and Alberto, 2002) to deal with an object that has the irregular shape such as a Convoluted shape. This feature is defined as the ratio of the maximum to minimum radius. That is

$$IR(S) = \frac{\max(\sqrt{(X_i - X')^2 + (Y_i - Y')^2})}{\min(\sqrt{(X_i - X')^2 + (Y_i - Y')^2})} \quad (6)$$

Equation (6) defines the ratio between the radius of the maximum circle enclosing the region and the maximum circle that can be contained within the region. Thus, a result will increase as the region spreads.

#### Boundary Irregularity

The irregularity of the boundary can usually report a cancer during its growth and propagation. For an evaluation, in this paper, divide the segment lesion into two sections, and then calculate the Euclidean distance between the centre of the lesion and all pixel's boundaries of each section separately. Finally, calculate the summation of the difference between two lesion parts, as shown in Fig. 6. The IR(S) method is based on calculating the Euclidean distance between the centre of the lesion and all pixels boundaries,

$$D_i = \sqrt{(x_2 - x_1)^2 + (y_2 - y_1)^2} \quad (7)$$

where  $x_2$  and  $y_2$  are the coordinates of the lesion's centre.  $x_1$  and  $y_1$  are the coordinates of pixel  $i$ .

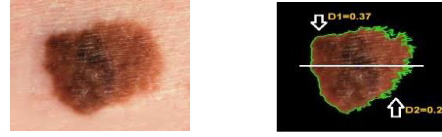


Fig. 6. (a) Original lesion image. (b) The two sections of the lesion according to the major axis divisions and the two distances values (D1 and D2).

#### 5.1.3 Color Index

One early sign of melanoma is the up-growth of color variations in area lesion colors. Because melanoma cells grow in pigment, they are often colorful around brown or black areas, depending upon the production of the melanin pigment at different depths in the skin (Sahil et al., 2016). Color index is calculated by converting the input image to HSV image value and then calculate the distance between each pixel's value in the lesion and the color we want to detect. The color index is an increment of 1, if the distance score is less than or equal to the pre-calculated threshold value. When the six colors (white, red, light brown, dark brown, blue-gray and black) are present, the maximum score is 6. The (8) is used to calculate the difference of  $\Delta E$  (Ihab, 2016).

$$\Delta E = \sqrt{(h_1 - h_2)^2 + (s_1 - s_2)^2 + (v_1 - v_2)^2} \quad (8)$$

Where  $h_1$ ,  $s_1$  and  $v_1$  are the components of the HSV colorimetric space of the desired color and  $h_2$ ,  $s_2$  and  $v_2$  those of each pixel of the image. The Fig. 8 shows the result  $C=4$  (red, light brown, dark brown and dark red).

#### 5.1.4 Diameter

Moles usually stay within certain size limits. A normal mole measures about six millimeters (1/4 inch) or less in diameter. Bigger moles can indicate signs of trouble. For calculating the horizontal and vertical dimensions of the lesion, in this paper, major axes length ( $h$ ) and minor axes length ( $v$ ) are used.

$$h = \max(i) - \min(i) \quad ; \quad v = \max(j) - \min(j) \quad (9)$$

Where  $(i, j)$  are the co-ordinates of all pixels located on the edge/border of the lesion. Then, approximately, the diameter is assumed to be the maximum value between  $h$  and  $v$ . Since the estimated diameter is pixels, it should be converted into millimeter unit by using the true size of the picture, to calculate the value of pixel in a millimeter, assume the pixel density is 96 dpi, there are 96 pixels per inch. Since 1 inch is equal to 2.54 cm. So there are 96 pixels per 2.54 cm. Than 1 pixel = (2.54 / 96) cm. Finally, there are **0.026 cm/pix** (0.26 mm/pix). The horizontal dimension of the lesion calculated by (Pavlos et al., 2007):

$$D = [(\text{major axes length} \times 0.26) / \text{image width}] \times 100 \quad (10)$$

In the example of Fig. 7, the major axes length=101 and image width=275, then the result of Diameter is 9.5 mm.



Fig. 7. Skin lesion (275×183jpeg image)

## 5.2 Classification

After obtaining the values of four components (Asymmetry, Border, Colors, and), then calculate TDV. The TDV is calculated based on the following formula where each one of the presented components is multiplied by a weighting factor:

$$TDV = 1.3 \times A + 0.1 \times B + 0.5 \times C + 0.5 \times D \quad (11)$$

This score is used to diagnosis benign, suspicious or melanoma skin lesion as presented as follows:

$$Diagnosis = \begin{cases} \text{Benign} & TDV < 4.75 \\ \text{Suspicious} & 4.8 < TDV < 5.45 \\ \text{Melanoma} & TDV > 5.45 \end{cases} \quad (12)$$

## 5.3 Extract Texture Feature

Image texture represents the spatial organization of intensity and color of an image, and it can be characterized in many different ways. In this paper, Gray Level Co-occurrence Matrix (GLCM) is used, this classic approach is based on computing the statistics features of the pairs of neighboring pixels, and can provide useful information about the spatial relationship of pixels of the gray-level. The GLCM is used to represent the texture of an image by calculating the statistical of repeated pairs of pixel with specific intensity values and in a specified spatial relationship occur in an image (Rashi and Saranjeet, 2015). In this paper, five statistical measures are extracted, Table 1 using in all the formulas  $P(i,j)$  denotes  $(i,j)^{th}$  entry or value in a normalized GLCM. The  $\mu_i$ ,  $\mu_j$ ,  $\sigma_i$ , and  $\sigma_j$  are the means and standard deviations of  $P_i$  and  $P_j$ :

Table 1. Texture Features.

Feature	Formula
Contrast	$\sum_{i,j}  i-j ^2 p(i,j)$
Energy	$\sum_{i,j} p(i,j)^2$
Homogeneity	$\sum_{i,j} \frac{1}{1+(i-j)^2} p(i,j)$
Correlation	$\frac{\sum_{i,j} (i-\mu_i)(j-\mu_j) p(i,j)}{\sigma_i \sigma_j}$
Entropy	$-\sum_{i,j} p(i,j) \log p(i,j)$

## 5.4 Extract Lesion Symptoms

Some of the symptoms and important data can be obtained from the patient for achieving an accurate and final diagnosis. These symptoms are divided into two types:

### 5.4.1 History of melanoma

- Date of lesion onset.
- Started gradually or suddenly.
- Pain, itching, oozing any discharge.
- Fever ( $\geq 38.6^\circ$  C), malaise nausea.
- Is this the first attack
- Occupation of a patient and Family history.

### 5.4.2 Palpation Examination

- Tenderness and temperature, the area around lesion is very warm.
- Boundary of lesion is smooth or solid.
- Mobility of lesions. If the lesion mole moves freely in all directions.

## 6. PROPOSED ALGORITHMS

6.1 Algorithm of preprocessing image is implemented in following steps:

- input the lesion image,
- Convert RGB color space into gray scale by forming a weighted sum of the R, G, and B components:  
$$0.2989 \times R + 0.5870 \times G + 0.1140 \times B,$$
- Apply the Gaussian filter on the gray scale image by using (2),
- Enhancement the result of the gray scale image, by performing the contrast stretch through using (1), and
- Finally compute the histogram equalization to the result of the image enhancement.

6.2 Algorithm for segmentation and Extract the connected Components lesion Object.

- input the result of enhancement lesion image,
- Calculate the threshold of the gray scale image by applying Otsu's method (Otsu, 2008),
- Convert the gray scale image into binary image based on threshold,
- Enhancement the result of the binary image by removes the small objects (area-size < 50 (pixel)), and
- Calculate the connected components of the objects from the binary image by applying (3).



6.3 Algorithm of extract the texture features is implemented in following steps:

- Input the lesion image after processing pre-process , segmentation and determine the lesion area,
- Convert RGB of lesion image to grey scale image,
- Compute four GLCM matrices for each direction ( $0^\circ, 45^\circ, 90^\circ, 135^\circ$ ) see (Nadia and Souhir, 2013),
- For each GLCM matrix computed the statistical features are present in Table 1.

7. EXPERIMENTS AND RESULTS

In this paper, all stages of the work are implemented in MATLAB R2016A with a set of 50 skin lesion images, which contains melanoma and benign skin images. Fig.8-(a) shows the original RGB image, fig.8-(b) represents the result of an image enhancement process after applying the Algorithm 6.1. After this, the segmentation and extract of the connected components lesion object algorithm have been applied on the grayscale intensity image. The desired segmented image is shown in Fig.8-(c). For each image, segmented lesion is surrounded by a solid blue line, and is determined by the centre of mass as shown in Fig.8-(d). The final segment is used to calculate the ABCD feature extraction values and statistics features.

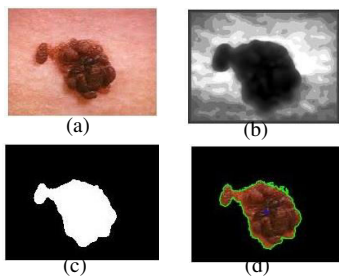


Fig.8. (a) Original RGB image; (b) Gray image (c) Segmented image after using connected component method.(d) Boundary tracing image and center of mass.

The experimental findings of ABCD features and statistics features extraction are discussing from the following sections:

A. Asymmetry index

The experimental results is shown that the values of asymmetry index of melanoma skin cancer fall within the values are greater than 0.20, as shown in Fig.9.

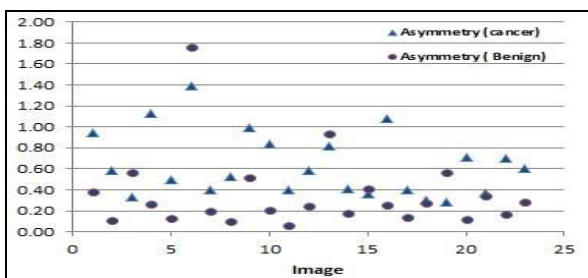


Fig.9. Asymmetry values for both melanoma and normal skin images.

B. Border Irregularity

The calculating of border irregularity index, in this paper, is based on representing three different measures:

- **Compactness C(S)**: It is calculated by using the (5). The experimental findings show that the values of C(S) of melanoma skin cancer fall between 0.11-0.6.
- **Dispersion Irregularity IR(S)**: It used to calculate border irregularity for all boundaries of the lesion. The IR(S) is calculated by using (6). The experimental results show that the values of IR(S) of melanoma skin cancer fall within the values greater than 0.10, as shown in Fig.10.
- **Boundary Irregularity**: The experimental results show that the values of boundary irregularity index of melanoma skin cancer fall within the values greater than 0.30, as shown in Fig.11.

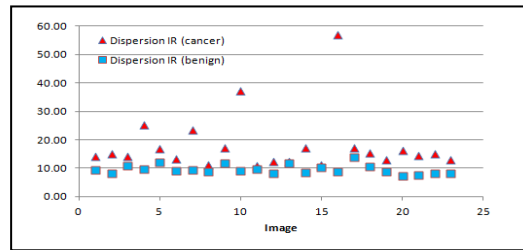


Fig.10. Dispersion irregularity values for both melanoma and normal skin images.

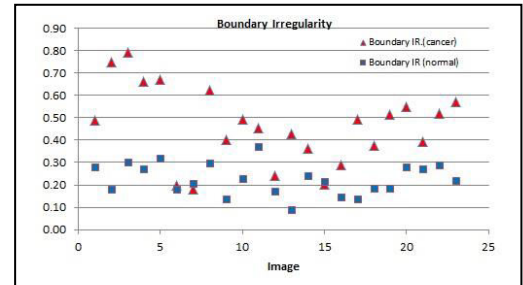


Fig.11. Boundary irregularity values for both melanoma and normal skin images.

C. Texture feature

The experimental results show that the values of contrast and entropy for benign skin images are less than the values of the same features of melanoma skin cancer, while the other features fall between the 0.1 and 1.0, as shown in Fig.12 and Fig.13 respectively.

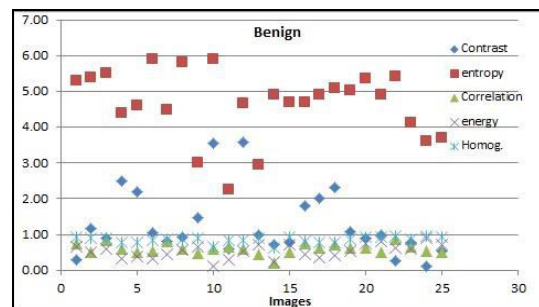


Fig.12. Texture features values for benign skin images.

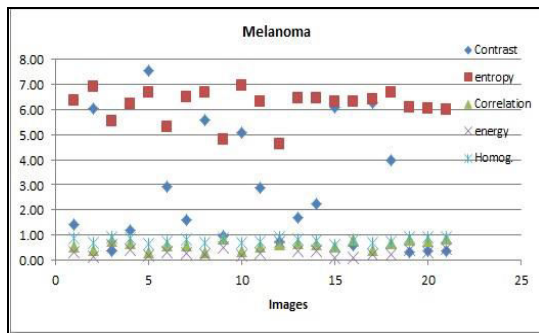


Fig.13.Texture features values for melanoma skin images.

The ABCD features, statistics features, and symptoms lesion are presented in The following GUI system

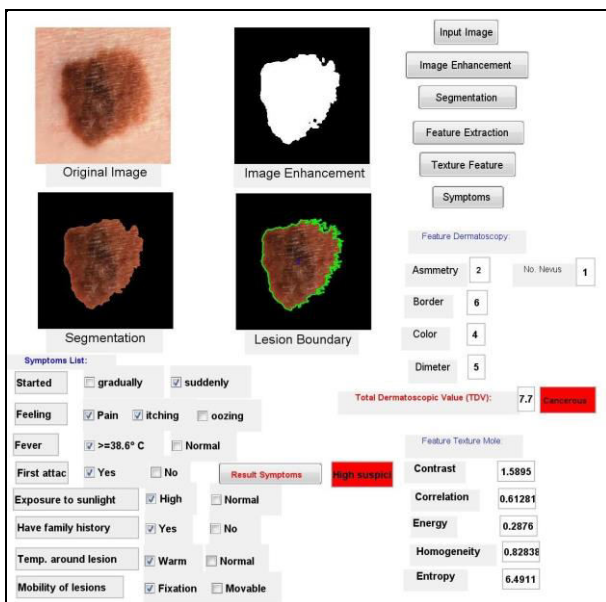


Fig.14. The GUI of the diagnosis melanoma skin cancer.

The performance of the developed system is evaluate by using accuracy gauge (13), and this research tested 50 images.

$$accuracy = \frac{\text{Number of detected lesions}}{\text{Number of images in the dataset}} \times 100 \quad (13)$$

## 8. CONCLUSIONS

The objective of this paper consists of the detection of melanoma based on three phases, ABCD rule of dermatoscopy, statistical texture analysis, and lesion symptoms. First conclusion boundary irregularity is a good indicator to determine the melanoma, as shown in Fig. 11. Another conclusion, there are some cases of melanoma, where the calculation of the asymmetry index of two different contents sections has been not large, because this method is based on the area (total pixel count of a lesion). The experiments showed that the contrast and entropy are powerful measurements in the characterization of the chaotic and variance of the cancerous skin images. Furthermore this system will be a great help for achieving an accurate final diagnosis, by using data of lesion symptoms and contribute the

symptoms with the rest phases. The experiment uses 50 cases of digital camera images, that contain both melanoma and benign skin images. Based on the experimental results, the accuracy of the development system is 90%

## REFERENCES

- Bilqis, A., Chastine, F. and Rahmat, M.W. (2010). ABCD Feature Extraction of Image Dermatoscopic Based On Morphology Analysis for Melanoma Skin Cancer Diagnosis. *Journal of Computer Science and Information*, vol. 3, pp. 82-90.
- Florence, T., Ernest, M. and Fred, N.K. (2011). An image-based diagnosis of virus and bacterial skin infections. *ICCIR*, 1-7.
- Geoff, D. (2009). *Digital image processing for medical applications*. Chapter 5, Cambridge, UK.
- Gleb, V.T. (2009). *Morphological Image Processing Basic concept*, Spring ELEN 4304/5365 DIP.
- Gopinathan, S. and Nancy, S. R. (2016). The Melanoma Skin Cancer Detection and Feature Extraction through Image Processing Tech. *Int. Journal of Emerging Trends & Tech. in Computer Science*, vol. 5, 106-112.
- Ihab, S.Z. (2016). Diagnosis of skin lesions based on dermoscopic image using image processing tech. *Int. Journal of signal processing*, vol. 9, 189-204
- Kaveri, E. and Chakravarthy, T. (2016). Skin Images Filtering Using Gaussian and Median Filtering Techniques. *IJIRCCE*, vol.4, pp.162-165.
- Mark, S. and Alberto, S.A. (2002). *Feature Extraction and Image Processing*; chapter 7, Newnes, Replika Press PVT Ltd.
- Nadia, S. and Souhir, B. (2013). A developed system for melanoma diagnosis. *Int. Journal of Computer Vision and Signal Processing*, vol. 3, pp. 10-17.
- Nilkamal, S.R. and Shweta, V.J. (2013). ABCD rule based automatic computer-aided skin cancer detection using MATLAB. *Int. Journal Computer Technology & Applications*, volume 4 (4), pp. 691-697.
- Otsu, N. (2008). A Threshold Selection Method from Gray-Level Histograms, *IEEE Transactions on Systems, Man, and Cybernetics*, vol. SMC-9, pp. 62-66
- Pavlos, L., Zaharias, D. Z., and Dimitra, G.K. (2007). Simple Matlab Tool for Automated Malignant Melanoma Diagnosis. *Article in: WSEAS Transactions on Info. Science and Applications*.
- Radu, D., Matei, D., Stefan, M. and Dan, P. (2010). Medical Images Classification for Skin Cancer Diagnosis Based on Combined Texture and Fractal Analysis. *WSEAS Transactions on Biology Biomedicine*, vol. 7, pp. 223-232.
- Rashi, G. and Saranjeet, S. (2015). Skin Cancer Detection Using GLCM Matrix Analysis and SVM Classifier. *International Journal of Applied Engineering and Technology*, vol. 5, pp. 6-11.
- Ravindra, P.S. and Manish, D. (2015). Histogram Equalization: A Strong Technique for Image Enhancement. *Int. Journal of Signal Processing, I.P. & Pattern Recognition*, vol. 8, pp.345-352.

Sahil, C., Sonika, J. and Bhavneet, K. (2016). Content based Image Retrieval using Selective Region Matching with Region of Interest and SVM. *Int. Journal of Computer Applications*, vol.137, pp.28-33.

Sanjay, J., Mehran K., and Vaishali, G. (2014). Skin Cancer Detection Using Digital Image Processing.

*International Journal of Scientific Eng. and Research*, vol. 3, 138-140

Santiago, R., and David A.G. (2016). Border and Asymmetry Measuring of Skin Lesion for Diagnostic of Melanoma Using a Perimeter Ratio. *Asian Journal of Computer Sc. and Inf. Technology*, vol.6, pp. 7-13.

# Temperature Data Logger for Industrial and Environmental Monitoring

Traian-Titi Șerban

University of Craiova (e-mail: tserban@electronics.ucv.ro)

---

**Abstract:** This paper presents a computerized instrument for temperature data logging using multiple sensor types. A versatile SCADA-like system able to display time sequences of the temperature evolutions of many measurement points is described. Based on a modular structure, the system allows for the temperature measurement using any of the main temperature sensors: thermocouples, RTD and analog output PTAT sensors. A specialized data acquisition microcontroller is used to convert the analog signals into digital data to be transmitted to a host computer that exhibits the user interface and displays the evolution of the temperature. The described system is dedicated to environment monitoring systems and to any industrial processes involving slow evolutions of temperature.

*Keywords:* temperature measurement, sensors, data logging, wireless data transmission

---

## 1. INTRODUCTION

With the increasing complexity of the control of industrial technologies and environmental processes monitoring, temperature measurement is the most common task. Because of changing measurement requirements, a versatile computerized system was designed, using the main temperature sensors and remote measurement.

The proposed system receives temperature information using basic sensors: thermocouples (TC), RTD (Resistance Temperature Detectors) and silicon integrated sensors (PTAT and/or PTCT). Their outputs are converted into voltages with normalized rated values using amplifiers and resistance-to-voltage (R/V) converters. These voltages are next converted into binary strings that are transferred to a PC to be displayed as time evolutions of the monitored temperatures. The system permits the process operator to detect any abnormal evolution and to take the most appropriate measures as fast as necessary to compensate the automated system failures.

The proposed system uses a simple RS-232 serial bus protocol, because in most industrial processes and in the natural environment the temperature variations are slow, but any of the faster modern data transfer protocols may be used instead.

The experimental model involved only few sensors of three types: two K-type thermocouples, two RTD (Pt100) and two LM35 silicon integrated sensors.

Thermocouples are used for wide temperature ranges, but their main drawbacks are the small output voltages and the need for compensation of the cold junction temperature.

RTD have a better linearity, a good temperature range, but need current sources and adequate adapters: passive bridge configurations, with excellent accuracies and

sensibilities but poor linearity, active bridges with excellent linearity but limited compatibility with the grounded sensors. Thermistors have an excellent sensibility but lower linearity and accuracy.

PTAT and PTCT silicon sensors are linear and sensible sensors but their temperature range is poor:  $-40\dots+150^{\circ}\text{C}$ .

The industrial applications involve restricted temperature ranges and usually more than one sensor type. The proposed versatile multipoint digital temperature measurement system include different modules for any temperature sensor type and a main board that converts the analog outputs of the adapters into digital words and transmits them to the PC to be displayed as time graphics on a wide screen.

## 2. SYSTEM DESIGN

The proposed system includes two sections (fig.1):

- a RTU-like remote module that includes:

- an analog section, with many analog adapter modules (AA) for different temperature sensors (TS); depending on the temperature ranges, thermocouples (TC), RTD (TR) or semiconductor sensors are used, followed by adequate adapters;

- a digital section, designed as mainboard, including a multichannel Data Acquisition System (DAS) that receives the analog signals from the previous adapters, converts them into digital words and transfers them as data by mean of a wireless link using a serial communication protocol ;

- a MTU-like unit including a PC, that receives data through a radio receiver and put them in a accesible form for the user running a specific program on Windows operating system.

Every analog module includes a temperature sensor, a low-pass filter as EMI/ESD rejector, and an output conditioner: thermocouple amplifier, resistance-to-voltage converter for RTD, or a level adapter for PTCT sensor. Similar systems are described in (Leung, 2015).

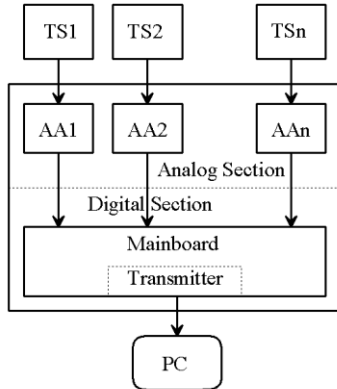


Fig. 1. Bloc Diagram of the Temperature Data Logger

The analog voltages on all channels are digitally converted with a single A/D and transmitted in the digital form to a PC that displays time evolutions of all supervised temperatures. Figure 2 shows the signal chain configuration including the radio transceivers.



Fig. 2. Block Diagram of a Measurement Channel

Similar structures are described in (Lepkowski, 2004)

### 2.1. The Analog Section

The analog adapters for the temperature sensors have several functions:

- rejection of the perturbations that affect the signals;
- conversion of the resistances into voltages;
- adjustment of the output voltages to match the next stages input ranges

Note that noise includes any low frequency disturbances other than continuous voltages representing the main signals (the outputs of the temperature sensors). That's why the rejections of the external noises are performed obtained using low-pass filters with a very low cut-off frequency. The same filters accomplish also the function of said anti-alias filters.

#### 2.1.1. The Thermocouples' Adapters

The adapter module for the thermocouple (K-type) was designed as an instrumentation amplifier to which a cold junction temperature compensation circuit. The standard three Op-Amp instrumentation amplifier configuration was used. Figure 3 shows the detailed schematic of a single thermocouple adapter. One can observe the final Op-Amp's multiple functions:

- summing amplifier for the output of the instrumentation amplifier and the cold junction compensation circuit;
- analog integrator (low-pass filter);
- general offset compensator.

The first stage of low-pass filtering includes passive RC pairs on both inputs to minimize the RFI and other high frequency interferences. The gain of the instrumentation amplifier may be adjusted during the module calibration. Cold junction temperature compensation circuit is designed assuming its low value, using the PTCT silicon sensor TC1047A and the recommendations described in (Lepkowski, 2004).

The thermocouple nonlinearity is compensated in the digital section's software using a look-up table correlated with the measurements' resolution (Ehinger, 2008).

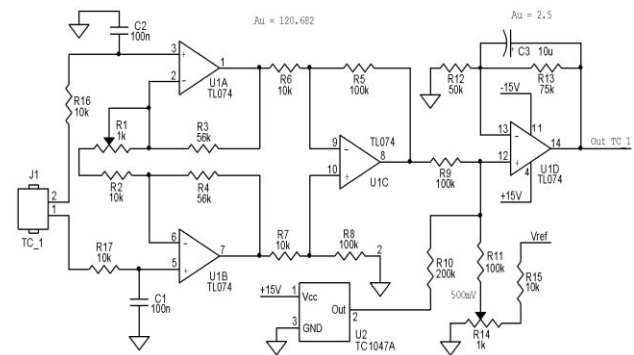


Fig. 3. Thermocouple Adapter (Instrumentation Amplifier)

The real dependencies  $u(\theta)$  of various thermocouples can be stored in the system's memory. For any digital output of the ADC the system identifies the corresponding temperature (from the input-output characteristic), so the linearity error is minimised.

#### 2.1.2. The RTD Adapters

Active bridge configurations (Wilson, 2005) minimise the linearity errors but in this approach only the signal wires' resistances were considered, requiring the four wires connection of the RTD to the R/V converters (figure 4). As the voltage drops across the RTD were high enough, not instrumentation but basic differential amplifiers were required to adapt the signals' levels to the inputs of the analog port of the digital section (U4).

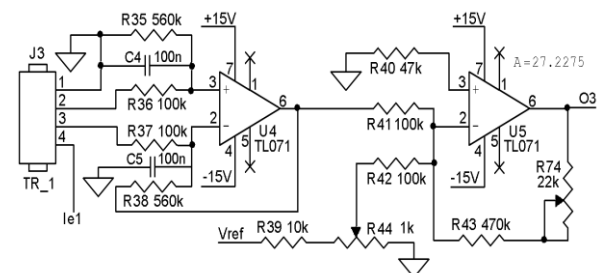


Fig. 4. RTD Adapter (R/V Converter)

The use of RTD for Celsius scale requires the offset of the differential amplifiers' output voltages with a constant reference level representing the output of the transducers

at 0°C. This was achieved by the second amplifier U5 in an inverting summing configuration. The actual position of R44 was determined during the calibration.

### 2.1.3. The RTD Current Sources

Another important module for the global accuracy of the data logger was the current source for the RTD (figure 5). The self heating conditions detailed in (Ehinger, 2008) were fulfilled by limiting the measurement current at 1mA in each RTD. A basic two channels adjustable current mirror driven by U11 (buffer for the adjustable reference voltage) was designed as bias current sources for the Pt100 RTD through the Ie1 and Ie2 outputs. R72, R73 were trimmed during the calibration (current setting).

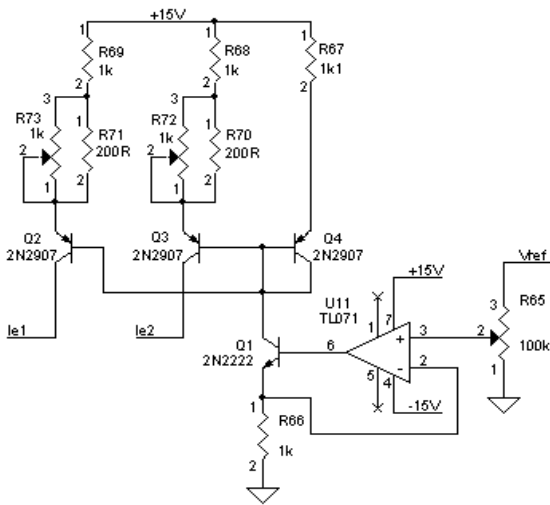


Fig.5. Dual Current Source for RTD

### 2.1.4. The PTCT Adapters

The PTCT adapters were designed as differential amplifiers with a fixed gain of 5, as illustrated in figure 6. Their functions are:

- the rejection of any voltage drops over the ground wires in the connection cables of the PTCT sensors;
- the maximization of the SNR providing the maximum resolution of the A/DC inside the microcontroller.

The potentiometer in figure 6 was needed for the initial offset cancellation during the calibration process.

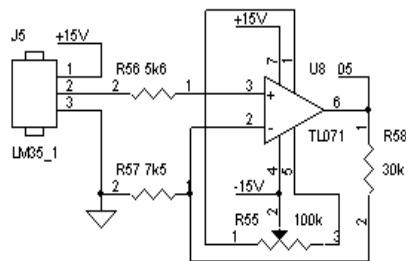


Fig.6. PTCT Sensor Adapter

### 2.2. The Digital Section

The detailed schematic of the digital section's first approach of the experimental model was based on a very

well known 8-bit microcontroller: PCB80C552 (U1) that includes an 8-channels built-in DAS, accessible through the analog port P0, as represented in figure 7. A mainboard was preferred in order to use the modern modular technology.

The 10-bit output of the A/DC ensures a 1:1000 relative resolution, meaning 0.1°C for the PTCT sensors in the range [0°C,102.3°C], 0.5°C for the RTD in the range [-50°C,462°C] and 1°C for the K-type thermocouples in the range [-100°C,+923°C]. Exhibited in two different registers, the output word requires a special reading routine to restore the correct order of the bits.

TL7726 clamp overvoltage protection integrated circuit (U7) on the input lines of the analog port P is a must for any analog inputs of microcontroller-based systems.

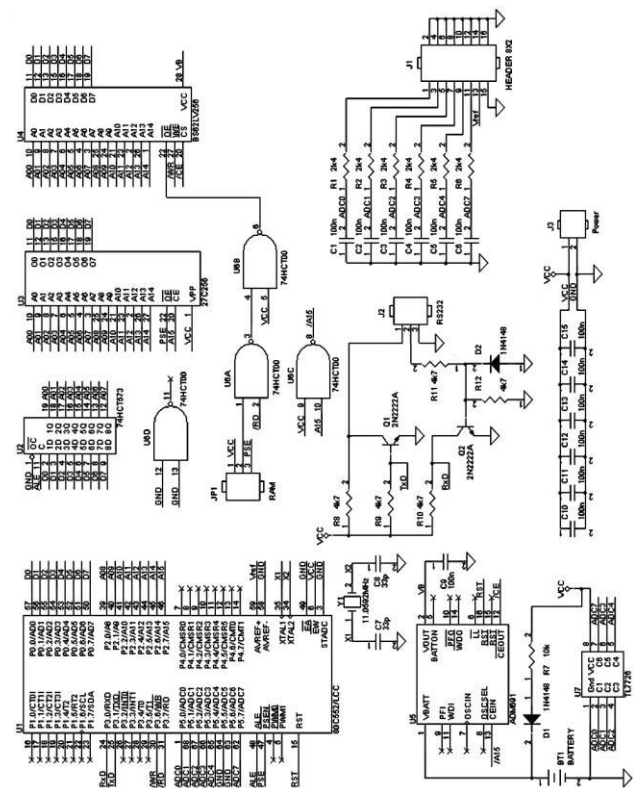


Fig.7. The Digital Section (First Approach)

Tests were performed using other development systems based on ATmega 328 (Arduino boards). Any of them offer at least 6 analog inputs fitting to the model. In most applications there is no need for the temperature measurement more than few times in a second, so analog multiplexers may be used in order to multiply the number of the channels (exp: using 4051 the number of the measured temperatures may be extended to least 48; using the 4067 one can get 96).

### 2.3. The Radio Transceivers

Data are transmitted to the host PC using a matched pair of HM-TR radio transceivers developed by Hope Microelectronics. As all the channels are sampled within a second (burst rate fixed using the internal T0 timer in the microcontroller), and next transmitted directly to the

PC, the simplex mode was sufficient. The transmitter module was mounted at the data output of the remote section of the measurement system, and the receiver - at the PC serial port COM1. Similar configurations are described in (Leung, 2015). The serial clock for transmission was generated using the second timer T1 in the microcontroller. Both transceivers were set for the 433MHz free band.

The connections were made following the schematics in figure 8. The standard UART interface was used in the schematic of the transmitter but no conversion of the TTL signals from the microcontroller was needed. In the second schematic (the receiver at the PC) the conversion TTL-RS232 was necessary for the COM1 port and achieved by using circuit MAX232.

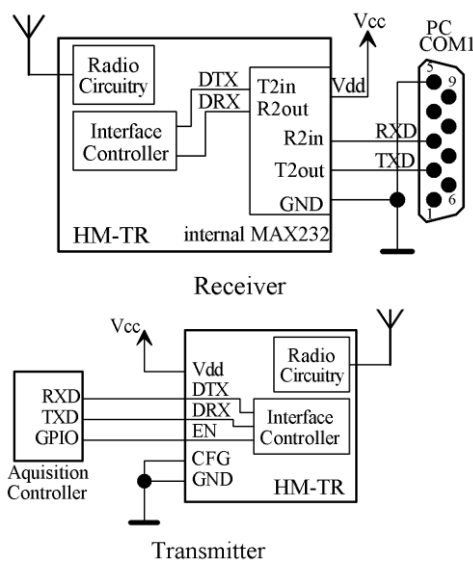


Fig.8. Radio Transceivers' Connections

## 2.4. Software

### 2.4.1. The Program in the Remote Unit

There are two components of the software, one for the microcontroller in the remote unit containing the analog interface and the other for the host PC.

The tasks of the microcontroller in the remote unit are:

- switching the analog multiplexer inputs in order to transfer the adapters' output voltages to the AD/C input;
- starting the A/D conversion;
- assembling and storing the A/DC output data;
- transmitting data to the host PC using a serial protocol

The routines included in the main program of the remote unit are:

- stack pointer setting;
- serial interface setting;
- T0 timer setting (1s acquisition burst clock);
- flags' resetting;

- presetting the intrinsic values in the used registers;
- enabling interrupt system;
- T0 timer starting;
- A/D converter control loop;
- serial transmitting loop;
- data transmission rate control

The A/D conversion control loop includes for every input channel the following operations:

- the selection command for the analog multiplexer;
- the A/D conversion start (in the appropriate mode);
- the EOC (end of conversion) signal is checked until 1;
- the pick-up of the output data of the A/DC;
- the transfer of the data to the memory;

These operations are repeated for every input channel selected in an acquisition burst.

The transmission loop includes the UART setting in the transmission mode followed by a sequenced 15-bytes package as follows:

- first 3 bytes – data package label (identified by the host PC as the beginning of data package);
- bytes 4 and 5 – value from the first semiconductor sensor;
- bytes 6 and 7 – value for the second semiconductor sensor;
- bytes 8 and 9 – value for the first RTD;
- bytes 10 and 11 – value for the second RTD;
- bytes 12 and 13 – value for the first TC;
- bytes 14 and 15 – value for the second TC

Every byte is separated by 110µs time gap to ensure that any possibility of overlapping is minimised.

Every interrupt generated by the timer T0 calls a transmission loop that counts the constant rate interrupts coming with every pair of bytes meaning the measured temperature values. The first channel is selected again, the flag is reset and the measuring loop is repeated.

The main program running in the microcontroller is built as a loop that begins with the test of the flag set by the timer T0 once per second, meaning that the measuring burst is finished. The flag is reset, the A/D conversion control followed by the transmission routines are called, so the measured values are transmitted to the host PC.

### 2.4.2. The Program in the PC

There are three parts of this program:

- setting routine;
- online display;
- options

All of them have visual interfaces using the OS windows. The program launch starts with the option for the channels' selection window and the time evolution of the temperature logging window.

The channels' selection window is represented in figure 9. One can select any or all of six channels as needed.

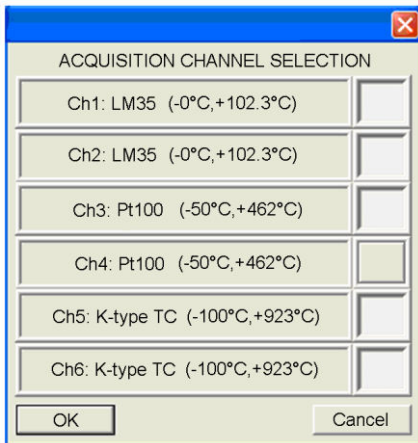


Fig.9. Channels' Selection Window

The operating system's resources are used as described in (Leung, 2015) for communication protocols.

The online display (logging) window shows the graphic representations of the evolutions and the numeric values of the measured temperatures. The window's refresh rate is 1s, as the data packets resulted in an acquisition burst are transmitted to the host PC. One can start, stop or exit the data logging using the appropriate buttons in the window.

For every measured temperature and for every acquisition burst, the point at the left of the screen representing the oldest acquired sample disappears and the whole graph is translated to the left, making room for the new point that is displayed at the right side of the screen. There are 500 points on the horizontal time axis for every temperature evolution, meaning that the recording of the last 500s of every measured temperature is always on the screen in the roll mode. For a more suggestive representation, lines were drawn between the points. Before completing the first 500s of recording, the time axis is scaled in autorange mode and these lines are more visible.

The vertical axis is scaled in Celsius degrees, also in autorange mode, with 0,2°C absolute resolution.

The measured temperatures are displayed in the values' space only for the selected channels and only when data packets are received from the remote unit. After the start command, the logging window remains unchanged until the first data package is received.

The program stops whenever the data transfer is unexpectedly interrupted.

Particular values are displayed few seconds in the values spaces for any selected point on any line representing the temperature evolution; next the roll mode is recovered and in the same spaces the current values are displayed.

Additional calculations may be performed by the microcontroller in the remote unit if higher precision is necessary. Particularly, when RTD are used onto large (including negative) ranges and absolute errors lower than 0,2°C are needed, the Calendar-Van Dusen equations must be used to estimate the actual measured value (Baker, 2003). The EN 60751 international standard exhibits the values for A, B, C constants used in the two formula corresponding to the positive and the (WIKA, 2016).

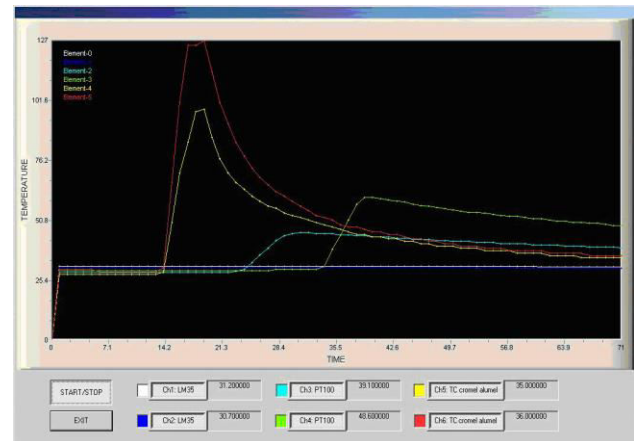


Fig.10. Temperature Logging Window

### 3. CONCLUSIONS

Most industrial technologies or environmental monitoring include multi-point temperature measurement in order to achieve automated control, advanced protection or corrective actions. A fully-functional experimental model was described to aid interested engineers. Only parts of the rated temperature ranges of the used sensors were considered for the model but the absolute resolutions were close to their known limits. Any improvements are possible and necessary in order to obtain application specific instruments with enhanced features.

The measurement environment must not exceed the EMI/ESD/EMC specifications. For this application there were no such imposed conditions, so these specifications were not considered for the used radio transceivers, neither for the system itself.

Further developments may include the control of the remote transmitters with mobile devices including Wi-Fi and cloud control. Actual advanced digital boards offer interface and computing capabilities to upgrade the described system. Containing all modules needed for the analog and digital signals' acquisition and wireless data transmission, Arduino Yún board may be the best fit for the digital section of the described system when used in Internet-of-Things or SCADA projects.



REFERENCES

- Baker, B. (2003). *Precision Temperature-Sensing With RTD Circuits*, Microchip Application Note AN687, ©Microchip Technology Inc.;
- Ehinger, K., Flach, D., Gellrich, L. et al. (2008) *Practices for Industrial Temperature Measurement*, ©2008 ABB Automation Products GmbH;
- Lepkowski, J. (2004). *Temperature Measurement Circuits for Embedded Applications*, Microchip Application Note AN929, ©Microchip Technology Inc.;
- Leung, H., Mukhopadhyay, S.C. (2015). *Smart Sensors, Measurement and Instrumentation, Vol. 13: Intelligent Environmental Sensing*, Springer, ISBN 978-3-319-12891-7;
- National Semiconductor (2008). *Temperature Sensor Handbook*, ©National Semiconductor Corporation, April 2008, [www.national.com/tempsensors](http://www.national.com/tempsensors);
- WIKA (2016). *Operating limits and tolerances of platinum resistance thermometers per EN 60751: 2008*, WIKA data sheet IN 00.17- 02/2016;
- Wilson, J. (2005). *Sensor Technology Handbook, Ch.20, Temperature Sensors*, ISBN 0-7506-7729-5, © 2005, Newnes, Elsevier Inc.

## Constrained Optimal Control and Feasibility Studies Performed for Landing Aircraft

George-Cristian Calugaru\*, Ionut Cristian Resceanu\*,  
Elena Andreea Danisor\*

\*University of Craiova, Faculty of Automation, Computers and Electronics (e-mails: calugaru.george.nds@gmail.com, resceanu@robotics.ucv.ro, andreea\_elenadanisor@yahoo.com)

**Abstract:** This article proposes an extension of the feasible sets theory in aircraft constrained optimal control problems. After a brief introduction in the constrained optimal control problem, its objective and the feasible solutions analysis, a case study for the proposed extension is presented which employs a model of an aircraft during the last phase of landing. Taken into account the specific parameters of model in the case study and for a given prediction horizon, the explicit controllers determined at each step together with the regions of the feasible partitions. Analyzing the feasible partitions under different use cases can present interest in design and development of aircraft systems which also employ model predictive control.

**Keywords:** aircraft control, constrained optimal control, model predictive control

### 1. INTRODUCTION

Optimization problems often are subject to several constraints which make up a system of inequalities. The solution set for such a system of inequalities is called the feasible set or the feasible region of the system.

In the last years, multiple studies have been conducted on determining or approximating feasible sets. Also, several MPC applications including an analysis of the characteristic feasible sets have been published.

For example, in (Yousefi et al., 2016), two-dimensional outer approximations of the feasible sets in wireless sensor networks are studied. The proposed method implies finding a tight polygon, which contains the target region and then obtaining the tightest ellipse in which the polygon is inscribed. This result is obtained by solving a convex optimization problem.

In (Gautam et al., 2013), the authors present the offline computation of the feasible sets for soft-constrained MPC systems. Basically, the approach implies softening of constraints for a class of MPC systems and relies on the use of an accurate penalty function so as to ensure that the solution to the problem is the same as the actual optimal solution when the MPC use case is feasible. Also, the penalty function should ensure that there is the minimum amount of constraint violations in case of infeasibility.

In (Gholami et al., 2013), the authors analyze the position of target nodes in cooperative wireless sensor networks which can be restricted to a number of feasible sets under specific conditions.

In (Costa et al., 2015), the authors study the feasibility of the optimization problem in the case a fault occurs. The

work studies the possibility of readjusting the constraints in a manner which eliminates the generated infeasibility.

Convex approximation of feasible set in NMPC is studied in (Grancharova et al., 2015).

Also, (Casini et al., 2014) studies feasible parameter set for linear models with unbounded uncertain regressors.

In (Zhou et al., 2013), the sample hold time effect on the feasible sets in model predictive design is studied. The purpose is to be able to select the sample/hold time accordingly avoiding infeasibility.

Even though the feasible sets and their impact in MPC systems have been studied thoroughly in the last period, a small limited number of studies have been carried out for aircraft control. Therefore this paper extends the feasibility analysis for aircraft control applications. The case study is based on the model of an aircraft during its last phase of landing. The constraints in this case are given by the actuator deflection angle, limited in this potential use case to  $1^\circ$ . Given these conditions, the feasibility regions are displayed for every step of a given prediction horizon. The analysis of the feasible sets can be of interest in the design and development of aircraft systems.

### 2. MODELS AND METHODS

#### 2.1 The constrained optimal control problem

Considering the linear time invariant system:

$$x(t+1) = Ax(t) + Bu(t) \quad (1)$$

where  $x(t) \in R^n$ ,  $u(t) \in R^m$  are the state and command variables which are subject to constraints:

$$x(t) \in X, u(t) \in U, \forall t \geq 0 \quad (2)$$

The sets  $X \subseteq R^n$  and  $U \subseteq R^m$  are polyhedra.

The objective function has the following form:

$$J_0(x(0), U_0) = p(x_{N_p}) + \sum_{k=0}^{N_p-1} q(x_k, u_k) \quad (3)$$

where  $x_k$  represents the state vector for step  $k$  obtained based on the initial state of the system:

$$x_{k+1} = Ax_k + Bu_k \quad (4)$$

with command sequence  $U_0 = [u'_0, \dots, u'_{N_p-1}]$ .

If the 1-norm or the  $\infty$ -norm are used in the objective function (3), then, [8]:

$$p(x_{N_p}) = \|Px_{N_p}\|_p$$

$$q(x_k, u_k) = \|Qx_k\|_p + \|Ru_k\|_p$$

with  $p=1$  or  $p=\infty$  and  $P, Q, R$  are full column rank matrices. The objective function (3) can be rewritten as:

$$J_0(x(0), U_0) = \|Px_{N_p}\|_p + \sum_{k=0}^{N_p-1} \|Qx_k\|_p + \|Ru_k\|_p \quad (5)$$

If the square of the Euclidian norm is used in the objective function (3), then  $p(x_{N_p}) = x'_{N_p} P x_{N_p}$  and  $q(x_k, u_k) = x'_k Q x_k + u'_k R u_k$ , with  $P \geq 0$ ,  $Q \geq 0$  and  $R \succ 0$ .

The objective function (3) can be further reshaped:

$$J_0(x(0), U_0) = x'_{N_p} P x_{N_p} + \sum_{k=0}^{N_p-1} x'_k Q x_k + u'_k R u_k \quad (6)$$

Considering the finite time constrained optimal control problem, (Borelli et al., 2014):

$$J_0^*(x(0)) = \min_{U_0} J_0(x(0), U_0) \quad (7)$$

With constraints:

$$x_{k+1} = Ax_k + Bu_k, \quad k = 0, \dots, N-1$$

$$x_k \in X, u_k \in U, \quad k = 0, \dots, N-1$$

$$x_{N_p} \in X_f$$

$$x_0 = x(0)$$

where  $N$  is the time horizon and  $X_f \subseteq R^n$  is a terminal polyhedral region.

Also,  $U_0 = [u'_0, \dots, u'_{N_p-1}] \in R^s, s = mN$  is the optimization vector. We denote by  $X_0 \subseteq X$  the set of initial states  $x(0)$  for which the optimal control problem (7) is feasible:

$$X_0 = \{x_0 \in R^n : \exists (u_0, \dots, u_{N_p-1})$$

$$x_k \in X, u_k \in U, k = 0, \dots, N_p - 1, x_{N_p} \in X_f,$$

where

$$x_{k+1} = Ax_k + Bu_k, k = 0, \dots, N_p - 1\}$$

If we use (6) for the square of the Euclidian norm and set:

$$\{(x, u) \in R^{n+m} : x \in X, u \in U\} = R^{n+m}, X_f = R^n$$

then problem (7) becomes the standard unconstrained optimal control problem in finite time, whose solution can be expressed through the time variant state feedback control law:

$$u^*(k) = F_k x(k), \quad k = 0, \dots, N-1 \quad (8)$$

The optimal cost is given by:

$$J_0^*(x(0)) = x(0)' P_0 x(0) \quad (9)$$

If  $N \rightarrow \infty$ , then problem (6), (7) and (9) becomes the standard LQR problem with infinite horizon for which the solution can be expressed as the state feedback control law:

$$u^*(k) = F_\infty x(k), \quad k = 0, 1, \dots \quad (10)$$

## 2.2. Feasible solutions

We note with  $X_i$ , the set of states  $x_i$  at time instance  $i$  for which the system (3) – (7) is feasible, for  $i = 0, \dots, N_p$ . The sets  $X_i$  play an important role in obtaining the solution for (7). There are 2 methods for defining and calculating  $X_i$ : the batch approach and the recursive approach. In the batch approach, Borelli et al. (2014):

$$X_i = \left\{ \begin{array}{l} x_i \in X : \exists (u_i, \dots, u_{N_p-1}) \\ x_k \in X, u_k \in U, k = i, \dots, N_p - 1, \\ x_{N_p} \in X_f, \\ x_{k+1} = Ax_k + Bu_k, k = i, \dots, N_p - 1 \end{array} \right\} \quad (11)$$

The definition of  $X_i$  from (11) requires that for every initial state there is a feasible command sequence  $U_i = [u'_i, \dots, u'_{N_p-1}]$  which ensures the evolution of the state within the bounds of the feasible set for the next time instances  $k = i+1, \dots, N_p - 1$  and also maintain  $x_N$  within  $X_f$  for instance  $N_p$ .

Given the state and command constraints sets  $X, X_f$  and  $U$  defined as H-polyhedra  $A_x x \leq b_x$ ,  $A_f x_N \leq b_f$ ,  $A_u u \leq b_u$ , the following polyhedron is defined :

$$P_i = \left\{ (U_i, x_i) \in R^{m(N_p-i)+n} : G_i U_i - E_i x_i \leq w_i \right\} \perp \perp (12)$$

where  $G_i$ ,  $E_i$  and  $w_i$  are defined as follows:

$$G_i = \begin{bmatrix} A_u & 0 & \dots & 0 \\ 0 & A_u & \dots & 0 \\ \vdots & \vdots & \ddots & \vdots \\ 0 & 0 & \dots & A_u \\ 0 & 0 & \dots & 0 \\ A_x B & 0 & \dots & 0 \\ A_x A B & A_x B & \dots & 0 \\ \vdots & \vdots & \ddots & \vdots \\ A_f A^{N_p-i-1} B & A_f A^{N_p-i-2} B & \dots & A_f B \end{bmatrix}$$

$$E_i = \begin{bmatrix} 0 \\ 0 \\ \vdots \\ 0 \\ -A_x \\ -A_x A \\ -A_x A^2 \\ \vdots \\ -A_f A^{N_p-i} \end{bmatrix} \quad w_i = \begin{bmatrix} b_u \\ b_u \\ \vdots \\ b_u \\ b_x \\ b_x \\ b_x \\ \vdots \\ b_f \end{bmatrix} \quad (13)$$

The set  $X_i$  is a polyhedron because it is the projection of polyhedron  $P_i$  in (12) and (13) on state space  $x_i$ .

In the recursive approach:

$$\begin{aligned} X_i &= \{x \in X : \exists u \in U, Ax + Bu \in X_{i+1}\}, \\ i &= 0, \dots, N_p - 1 \\ X_{N_p} &= X_f \end{aligned} \quad (14)$$

The definition of  $X_i$  in (14) is recursive and needs that for every feasible initial state  $x_i \in X_i$  there is a feasible command  $u_i$  which maintains the next state  $Ax_i + Bu_i$  within the bounds of the feasible set  $X_{i+1}$ . It can be written in a more compact form like below:

$$X_i = \text{Pr}e(X_{i+1}) \cap X \quad (15)$$

Initializing  $X_{N_p}$  with  $X_f$  and solving (14), the same  $X_i$  sets are obtained as with the batch approach. This

recursive method can lead to an alternative approach for determining the  $X_i$  sets.

Given  $X_i$  an H-polyhedron  $Ax_i x \leq bx_i$ . Then the set  $X_{i-1}$  is the projection of the next polyhedron on state space  $x_i$ :

$$\begin{bmatrix} A_u \\ 0 \\ Ax_i B \end{bmatrix} u_i + \begin{bmatrix} 0 \\ Ax_i A \end{bmatrix} x_i \leq \begin{bmatrix} b_u \\ b_x \\ b_{x_i} \end{bmatrix} \quad (16)$$

Considering the problem (14). The set  $X_0$  is the set of all initial states  $x_0$  for which (14) is feasible. A command sequence  $\bar{U}_0 = [\bar{u}_0, \dots, \bar{u}_{N_p-1}]$  is feasible for (14) only if for all the time instances  $i$ , the state  $x_i$  obtained through applying  $\bar{u}_0, \dots, \bar{u}_{i-1}$  to system model  $x_{k+1} = Ax_k + Bu_k$  with the initial state  $x_0 \in X_0$  belongs to  $X_i$ . Also,  $X_i$  is the set of feasible initial states for the problem below:

$$J_i^*(x(0)) = \min_{U_i} p(x_{N_p}) + \sum_{k=i}^{N_p-1} q(x_k, u_k) \quad (17)$$

with constraints:

$$\begin{aligned} x_{k+1} &= Ax_k + Bu_k, k = i, \dots, N_p - 1 \\ x_k &\in X, u_k \in U, k = i, \dots, N_p - 1 \\ x_{N_p} &\in X_f \end{aligned}$$

**Theorem.** Given the set of terminal state constraints  $X_f$  equal with  $X$ . Then, (Borelli et al., 2014):

1. The feasible set  $X_i$ ,  $i = 0, \dots, N_p - 1$  is equal to the controllable set for  $(N_p - i)$  steps:  
 $X_i = K_{N_p-i}(X)$
2. The feasible set  $X_i$ ,  $i = 0, \dots, N_p - 1$  contains the maximal invariant command set:  $C_\infty \subseteq X_i$
3. The feasible set  $X_i$ , is command invariant if and only if the maximal invariant command set is finite determined and  $N_p - i$  is greater or equal with its rank  $\bar{N}$ :

$$X_i \subseteq \text{Pr}e(X_i) \Leftrightarrow C_\infty = K_{N_p-i}(X),$$

$$i \leq N_p - \bar{N}$$

4.  $X_i \subseteq X_j$ , if  $i < j$  for  $i = 0, \dots, N_p - 1$ . The size of the feasible set  $X_i$  no longer decreases if and only if the maximal invariant command set is finite determined and  $N_p - i$  is greater than its rank:  $X_i \subset X_j$  if  $N_p - \bar{N} < i < j < N_p$ . And  $X_i = C_\infty$ , if  $N_p - \bar{N}$ .

**Theorem.** Given the set of terminal state constraints  $X_f$ , an invariant command subset of  $X$ . Then, (Borelli et. al., 2014):

1. The feasible set  $X_i$ ,  $i=0, \dots, N_p-1$  is equal with the stabilizing  $(N_p-i)$  step set:  
 $X_i = K_{N_p-i}(X_f)$
2. The feasible set  $X_i$ ,  $i=0, \dots, N_p-1$  is command invariant and contains the maximal invariant command set  $X_i \subseteq C_\infty$
3.  $X_i \supseteq X_j$ , if  $i < j$ ,  $i=0, \dots, N_p-1$ . The size of the feasible set  $X_i$  is no longer increasing if and only if the maximal stabilizing set is finite determined and  $N_p-i$  is greater than its rank:

$$X_i \supset X_j, \text{ if } N_p - \bar{N} < i < j < N_p \text{ and:}$$

$$X_i = K_\infty(X_f) \text{ if } i \leq N_p - \bar{N}.$$

### 3. CASE STUDY

#### 3.1. Aircraft model

The feasibility studies proposed in this paper are based on a model of an aircraft during its last phase of landing, as given in, (Iancu et. al., 1999):

$$\begin{cases} \dot{\omega}_y(t) = -0.6\omega_y(t) - 0.76\Theta(t) + 0.003w(t) + 2.34u_p(t) \\ \dot{\Theta}(t) = \omega_y(t) \\ \dot{w}(t) = 102.4\Theta(t) - 0.4w(t) \end{cases} \quad (18)$$

The variables used have the following meaning:

- $\omega_y(t)$  - pitch angle rate
- $\Theta(t)$  - the pitch angle
- $u_p(t)$  - command of the actuator for the horizontal rudder
- $w(t)$  - altitude rate

The actuator for the horizontal rudder is taken into account in the model. In order for an accurate landing procedure, the flight program must take into account the following parameters:

- Plane altitude in this phase is 30 m
- The plane's horizontal speed is 77 m/s
- Roll and yaw movements have already been stabilized
- The descending speed up to the point of 30 m is  $w_0 = -6m/s$
- The pitch angle in this phase must be at most  $2^\circ$ .

- The descending speed must be at most 0.6 m/s exactly in the moment when the plan touches the runway surface, otherwise the landing gear can be susceptible to damage.
- The landing phase lasts for 20 sec
- The landing trajectory is given by:

$$h(t) = \begin{cases} 30e^{-t/5}, & 0 \leq t \leq 15 \\ 6-t, & 15 < t \leq 20 \end{cases} \quad (19)$$

- The descending speed reference is:

$$w(t) = \dot{h}(t) = \begin{cases} -6e^{-t/5}, & 0 \leq t \leq 15 \\ -1, & 15 < t \leq 20 \end{cases} \quad (20)$$

The mathematical model shows an unstable object, this being shown also by the eigenvalues:

$$\begin{aligned} \lambda_1 &= -0.5016 + j0.8670 \\ \lambda_2 &= -0.5016 - j0.8670 \\ \lambda_3 &= 0.0032 \end{aligned} \quad (21)$$

In the control structure initially proposed in (Iancu et al., 1999), a partial state feedback loop is introduced (for  $\omega_y$  and  $\Theta$ ) and also a feedback loop for the output  $w$ . This can be seen in Fig. 1 below.

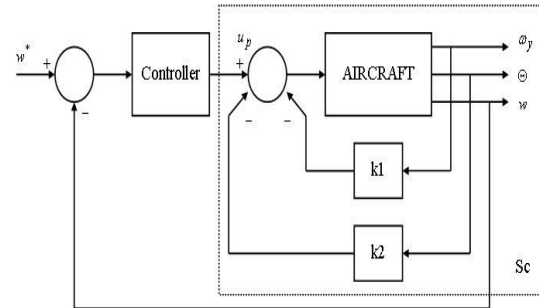


Fig.1. Control system with a partial state feedback ( $\omega_y$  and  $\Theta$ ) and a feedback loop for the  $w$  output;  $S_c$  - the compensated system as presented in (Iancu et al., 1999)

Considering the state variables, a feedback loop is constructed, with the matrix  $K$  obtained with the LQR algorithm, Iancu et al. (1999):

$$J = \int_0^\infty [x^T(t)Qx(t) + u^T(t)Vu(t)] dt \quad (22)$$

$$K = V^{-1}B^T P \quad (23)$$

$P$  - matrix for the solution of the Ricatti algebraic equation:

$$PA + A^T P - PBV^{-1}B^T P + Q = 0 \quad (24)$$

The compensated system imposes the following eigenvalues:

$$\begin{aligned} \lambda_1^* &= -8.1072 + j7.4184 \\ \lambda_2^* &= -8.1072 - j7.4184 \\ \lambda_3^* &= -0.3973 \end{aligned} \quad (25)$$

The feedback matrix  $K$  is given by:

$$K = [6.5761 \quad 50.5295 \quad 0] \quad (26)$$

The state space representation of the compensated system is:

$$A = \begin{bmatrix} -0.6 & -0.76 & 0.003 \\ 1 & 0 & 0 \\ 0 & 102.4 & -0.4 \end{bmatrix} \quad (27)$$

$$B = \begin{bmatrix} 2.374 \\ 0 \\ 0 \end{bmatrix} \quad C = [0 \quad 0 \quad 1] \quad D = 0$$

Based on (27), an equivalent model can be calculated for the compensated system:

$$A_e = A - BK \quad (28)$$

This equivalent model is the basis for the proposed feasibility studies.

### 3.2. Simulations

For the purpose of the analysis we employ the model of the plane during its last phase of landing as presented above. The aim is to determine the optimal controller which solves the problem (7) with  $p = \infty$ ,  $N = 3$ ,  $P = I_3$ ,  $Q = I_3$  and  $R = 0.8$ , with the command constraints (which can be assimilated to a limitation on the actuators of the aircraft control surfaces):

$$U = \{u \in R : -1 \leq u \leq 1\} \quad (29)$$

And the command constraints:

$$X = \left\{ x \in R^3 : \begin{bmatrix} -10 \\ -10 \\ -10 \end{bmatrix} \leq x \leq \begin{bmatrix} 10 \\ 10 \\ 10 \end{bmatrix} \right\} \quad (30)$$

The explicit controllers determined for each step of the prediction horizon are represented in the figures below:

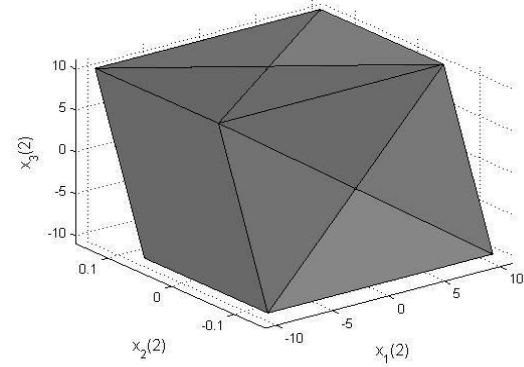


Fig. 2 The explicit controller and the corresponding regions for  $N_p = 3$  (24 regions)

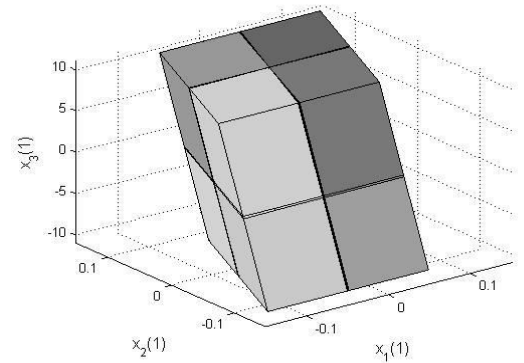


Fig. 3. The explicit controller and the corresponding regions for  $N_p = 2$  (64 regions)

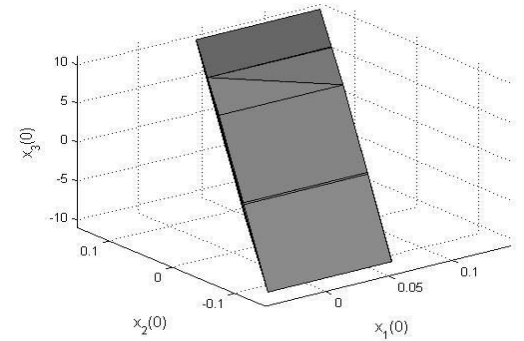


Fig. 4. The explicit controller and the corresponding regions for  $N_p = 1$  (19 regions)

Example of a feasible partition for the third controller:

$$\begin{bmatrix} 0 & -0.7071 & 0.7071 \\ 0 & 0 & -1 \\ 0 & -1 & 0.0039 \\ 0.8575 & 0.5145 & -0.002 \\ -0.9285 & 0.3714 & -0.0015 \end{bmatrix} \leq \begin{bmatrix} 0 \\ 10 \\ 0.0977 \\ 0 \\ 0 \end{bmatrix} \quad (31)$$

#### 4. CONCLUSIONS

This paper has analyzed an extension of the computational of feasible sets for aircraft control applications. The model used is that of an aircraft during its last phase of landing. The use case of the analysis implies adding a constraint on the actuator deflection of  $1^\circ$ . In this case, for a prediction horizon of  $N_p = 3$  the distribution of feasible regions is shown for the selected model. The purpose of this paper is to show the necessity of feasibility studies in aircraft applications with the selection of as many specific conditions as possible (to cover every possible occurrence on infeasibility). The computations of feasibility sets for MPC applications can be of interest in design and development of aircraft systems.

#### REFERENCES

- Borrelli, F., Bemporad, A., Morari, M. (2014), Predictive Control for linear and hybrid systems, MPC lab at UC Berkeley
- Casini, M., Garulli, A., and Vicino, A. (2014), Feasible Parameter Set Approximation for Linear Models with Bounded Uncertain Regressors, in *IEEE Transactions on Automatic Control*, vol. 59, no. 11, pp. 2910-2920.
- Costa, D.E.S., Galvão, R.K.H., de Almeida, F.A and Afonso, R.J.M. (2015), Improving fault tolerance in model predictive control through enlargement of the recursively feasible set, *2015 European Control Conference (ECC)*, Linz, pp. 3059-3065.
- Gautam, A., and Soh, Y.C. (2013), Soft-constrained model predictive control based on off-line-computed feasible sets, *52nd IEEE Conference on Decision and Control, Firenze*, pp. 5777-5782.
- Gholami, M.R., Wymeersch, H., Gezici, S., and Strom, E.G. (2013), Distributed Bounding of Feasible Sets in Cooperative Wireless Network Positioning, *IEEE Communications Letters*, vol. 17, no. 8, pp. 1596-1599.
- Grancharova, A., and Olaru, S. (2014), Explicit interpolation-based nonlinear model predictive control with a convex approximation of the feasible set, *2014 IEEE Conference on Control Applications (CCA)*, Juan Les Antibes, pp. 1824-1830.
- Iancu, E., Vinatoru, M. (1999), *Detectia si localizarea defectelor in sistemele dinamice*, Ed. Universitaria, Craiova, Romania, 1999.
- Yousefi, S., Wymeersch, H., Chang, X.W. and Champagne, B. (2016), Tight Two-Dimensional Outer-Approximations of Feasible Sets in Wireless Sensor Networks, in *IEEE Communications Letters*, vol. 20, no. 3, pp. 570-573.
- Zhou, D., and Ling, K.V. (2013), The effect of sample/hold time on initial feasible set in model predictive control design, *2013 Australian Control Conference*, Fremantle, WA, pp. 212-217.

## Integration of metrology principles in the next generation of ERP using SAP Fiori interface, collaboration, SaaS and SOA

Viorel Costin Banța, Dorian Cojocaru

*Mechatronics and Robotics Department, Faculty of Automation, Computers and Electronics,  
University of Craiova, Romania (e-mail: bantaviorel@gmail.com)*

---

**Abstract:** The paper deals with what the Internet offers in order to connect our ERP systems, using mobility and SAP Fiori interface, with actual business context. With this article we want to covered some aspects in order to show how metrology principles are integrated with an Enterprise Resource Planning (ERP) systems, how we can have utilized the interface SAP Fiori - for mobility purposes, through enabled learning organization and software as a service. The authors have been focused to describe, discuss and show the methodology of development of a metrology software application included in e-metrology category for the calibration of oil tanks. For this have been used the new technologies from SAP - WebDynpro, SAP Fiori interface, implemented and tested in a gas and oil business environment. The existing ERP - SAP in fact, which is the environment for the application, is installed in the oil and gas company, this means that our application is integrated with all processes existed in area of Demand Management environment. The development / programming of the CRT application was done using the ABAP programming environment, using WebDynpro technology as a Web-oriented programming method. All necessary phases (analysis, testing and implementation) were part of the entire development agreed methodology for our software CRT tool. The CRT application for calibration management was tested in the E&P and Marketing divisions of an oil and gas company, this article highlighting the extension to the mobility of the application using the SAP Fiori interface.

**Keywords:** SAP Fiori interface, SOA, SaaS, e-Metrology System, ERP III, Enabled Learning Organizations, Calibration, ERP

---

### 1. INTRODUCTION

When we discuss about an ERP we have to take into considerations a system which facilitated integrated and real-time planning, customer response, production and client response. On the other hand, ERP is oriented to management of the processes existing in all divisions that are part of companies which has install such an integrated system. It is known that this type of system known to use multilingual capabilities, to recognize multicurrency handling ability, to use the legal environments existing in each country and tax reporting papers.

In 1990, Gartner Group has introduced this new concept – “ERP - Enterprise Resource Planning” in order to define and manage manufacturing resource planning, this new concept was named MRP II, which fill in the gap resulted by the evolution of the integrate applications versus manufacturing area. This new concept, MRP II, was in fact a method designed to help the companies involved, to plan all resources, without limitations, application environment, skills of the users and capabilities of used computers (Keller, 1999), (Chen and Lin, 2008), (Leu and Huang, 2009), (Lin and Shih, 2009). That new concept was coming with a lot of benefits: in order to increase the performance of the productivity in the concept was

mentioned that the resources have to be managed simple (Peter and Pohl, 2009). The business process management was improved when ERP arrived, so overall, this concept was used to improve business activities, in fact all activities were integrated, from all divisions, which were part of a company. The companies Oracle, Microsoft and SAP were and are the main actors in this field. In 1972 Germany, SAP started this activity in order to produce software (initial purpose was to offer to the customers this possibility to interact with a single database – company database) and, now, is the major enterprise software company in the ERP world. This concept, ESR (Enterprise Services Repository) is the concept which comes with the definition of the central repository information. This information is used in SAP NetWeaver platform, and this is a callable application using services and is integrated with other applications used by the business (Banta and all, 2012), (Banta and Cojocaru, 2013), (Banta and Cojocaru, 2014).

Regarding our point of view, from authors perspective, for this article, the major aspect was creating and integrate a Z application (in terms of SAP), a homemade application using the existing ERP – SAP and to improve the possibility to use this application on mobility platform, the entire software uses as a database an IBM product, DB6,



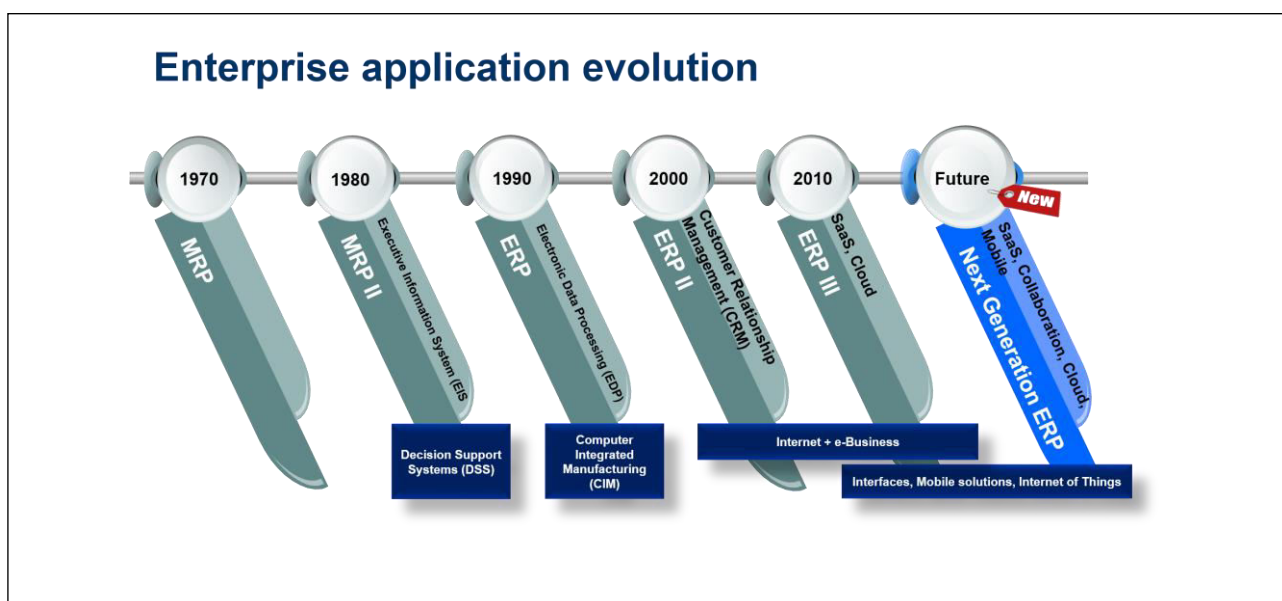


Fig. 1 Evolution of enterprise application systems

the year 1970 was the beginning for this product (Banta and Cojocaru, 2014), (Banta and all, 2014).

## 2. SOFTWARE REQUIREMENTS SPECIFICATION, METHODOLOGIES FOR CALIBRATION OIL TANKS

The next step for ERP is to integrate other new trends, the promises for standardizations of ERP is to add concepts like SOA (Service Oriented Architecture), SaaS (Service as a Software) and Learning Collaboration, so we can figure this like a steps from ERP to ERP II and now to ERP III (Peter and Pohl, 2009), (Lin and Shih, 2009), (Banta and Cojocaru, 2014). More than that according with the actually trends, we already started to adapt our configuration (e-metrology system), to the mobility standards, using SAP Fiori interface which can help us in this way. For our z-metrology application, when we start to use SAP Fiori, was a new user-experience (UX) for everything regarding SAP software and application, for our colleagues from the business area. For that reason, we keep our application, for calibration reservoirs, but we change the interface which access this SAP z-module in order to create a functional specification designed to help us to create a proper view of the entire environment, so, more or less the users can access this tool from the office or from the outside of the office (via mobile, tablet). We create a community, in upstream team (former Exploration, Production area and Marketing area) which give us a lot of hints about calibration (tank calibrations: vertical or horizontal) (Peter and Pohl, 2009), (Lin and Shih, 2009), (Banta and all, 2012). When we start to develop this kind of CRT application, we choose to use ESR (Enterprise Services Repository - ES Repository). This is a component. In fact, it is an add-on which is installed in SAP NetWeaver environment. This SAP add-on, in fact ESR, can support a model of development which manage to top down enterprise service development

in both cases: provisioning and consuming (services) (Peter and Pohl, 2009). In the open discussions about support, this ESR add-on can do point-to-point services consumption in the SAP NetWeaver system landscape (Dev-Qas-Prd). This add-on, which is delivered by SAP, helps the customers to use more and more the enterprise services and the utility of this approach type. In order to define proper enterprise service, data types or other related design objects, SAP ESR is capable to provide modeling environment for this kind of models/data. Another point which is a plus for this facility offered by SAP via ESR is the possibility to easy design models and maintain service interfaces (in our case the interface between recording system for calibration and our z-module created in SAP) (Peter and Pohl, 2009). Regarding our particular case, in fact the development of a Z-module for calculations and print all needed legal papers, results received from a calibration of a reservoir, for this reason a global data type catalogue is needed. This catalogue is based on core technical components, specifications standard in order to ensure a high degree of reusability of modifications. Even here we add the possibility to archive the document based on barcode, actually when an inspector goes to the reservoir place, he will take with him all legal printed papers with a barcode, and when he will come back, he will scan this papers and will upload all to the same inspection created before base on the same barcode.

SAP Fiori is a part of innovations on SAP side, so SAP comes every year with a lot of new things, this means that the customers can and will try to adapt these new capabilities in their area, therefore, in our exploration and production field (and now in Marketing – filling stations), the aim is to automate and simplify processes in order to have a visibility and traceability of our modifications and to adapt several changes quickly and with improved results (Lin and Shih, 2009), (Banta and all, 2012). For this reason, a lot of oil and gas companies create technical teams (development and workflow), these teams are

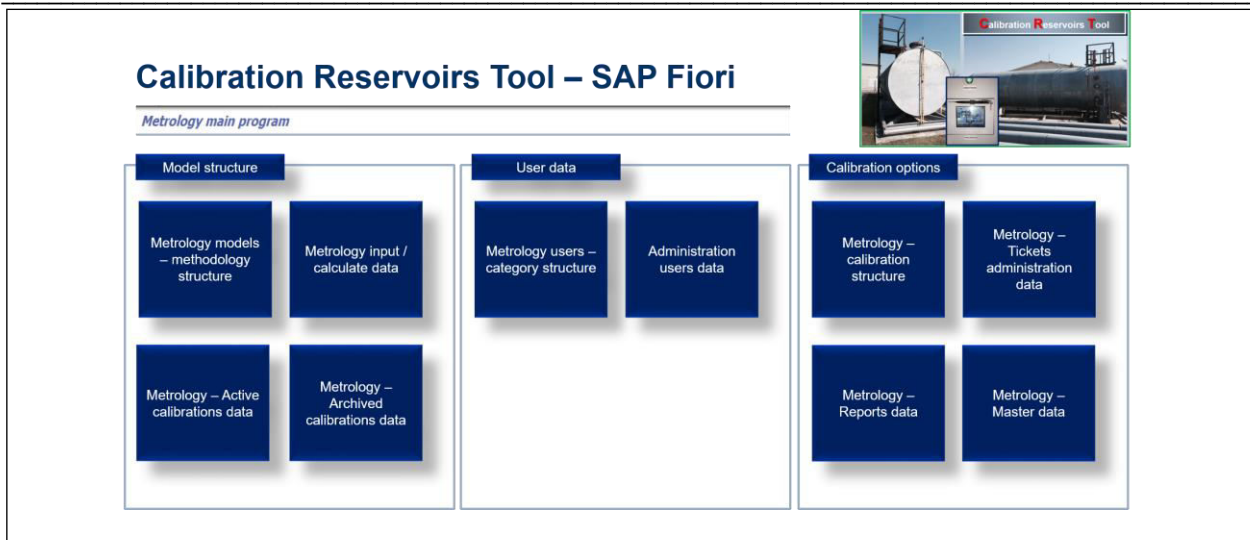


Fig. 2 Evolution of CRT to SAP Fiori interface - new UX experience

assigned to help and solve the technical problems of each specific department (SAP Technology Center - inside Enterprise Application Service Line - in fact Technology Department). This teams, Development and SAP Cross Technologies, supports everything regarding adaptations, modifications / developments, even if is standard one or developed inside, means z-modifications (Lin and Shih, 2009), (Banta and Cojocaru, 2013), (Banta and all, 2014). In another hand these teams (SAP Cross Technology team and Development team) are involved, together with functional consultants, to provide best practices regarding all known processes – technical, development and functional (metrology case studies) in order to improve the functionality and the results acquired.

In another hand these teams (SAP Cross Technology team and Development team) are involved, together with functional consultants, to provide best practices regarding all known processes – technical, development and functional (metrology case studies) in order to improve the functionality and the results acquired. In the oil and gas company where the CRT tool/application exists, all ABAP modifications were stored, so the SAP standard adaptations and the customer improvements, were triggered via a Z tool – named Development Center tool (DC). All this ABAP activities (objects modifications, adaptations) were kept inside SAP Solution Manager, where all z-programs of DC and configuration / customizations was stored (Lin and Shih, 2009), (Banta and Cojocaru, 2013), (Banta and all., 2014).

Our scope was to create a customer tool which will have the main task, storing data coming from calibration process (oil reservoirs - using legal methods) and using adaptive algorithms, the calculation of needed data for calibration certificate. These data are stored in customer z-tables, having connections with standard tables (in.: user table, security/authorization table, fixed assets table, etc.) (Banta and Cojocaru, 2013), (Banta and all., 2014).

Now after some years our task is to modify and adapt our tool to SAP innovations which contribute to a user innovative interface for our colleagues from business side. The innovation from SAP, Fiori in fact, can offer this and for that reason we already made an adaptation for our application, this means that our tool will be used using mobile or tablets. Our tool/application - CRT named - was created based on a technical case study from business side – marketing and exploration/production area. From legal and technical aspects, this tool full fills all calibration requirements for oil reservoirs/tanks – for metrology area (BRML, 2002). In our business areas, marketing and E&P, two types of tanks/reservoirs are used: horizontal and vertical (Fig. 3 and Fig. 4).



Fig. 3 Horizontal oil reservoir

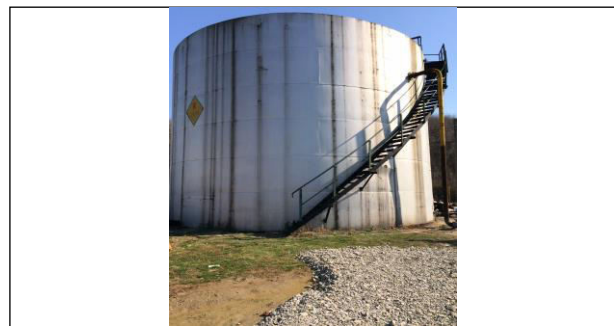


Fig. 4 Vertical oil reservoir

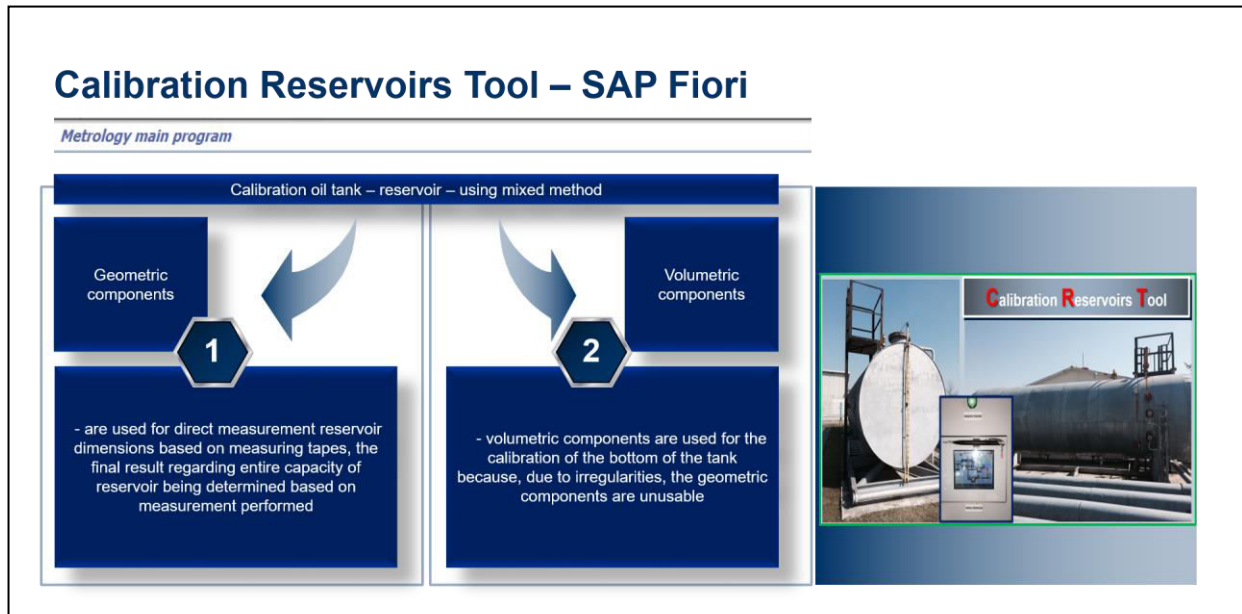


Fig. 5 Mixed method - components

According with specific FS (functional specification) that was created together with technical people (engineers from maintenance department – business community), the development was started, in order to achieve the final target: legal calibration paper (calibration certificate) inside SAP, with a z-module, developed internally with resources provided by SAP Technology Department - development Center team (DC) and according with “BRML legal rules”, (Banta and Cojocaru (2013)), (Banta and all (2014)).

Our article, will refer to a calibration for on oil tank/reservoir which is used in marketing and E&P areas.

The used method is mixed method (volumetric and geometric components are needed) (Fig. 5). The case study contain real data collected from the territory, based on needed information in order to complete the calibration file (Jardim-Goncalves and all (2012)), (Bavaraju (2016)), (Goebels and all (2016)). Our final scope is to calibrate a reservoir (vertically cylinder reservoir), with fixed roof and we have to know that this reservoir cannot be, nominal capacity, bigger than 40 cubic meters (BRML (2007)). It is known that for reservoirs that have obvious deformity the mixed method cannot be used, even for reservoirs which the circular horizontal section doesn't appear. We use, in our test case, some metal measurements unit (with overflow), as we have following described: 100, 200, 500 dm<sup>3</sup>, or in other cases

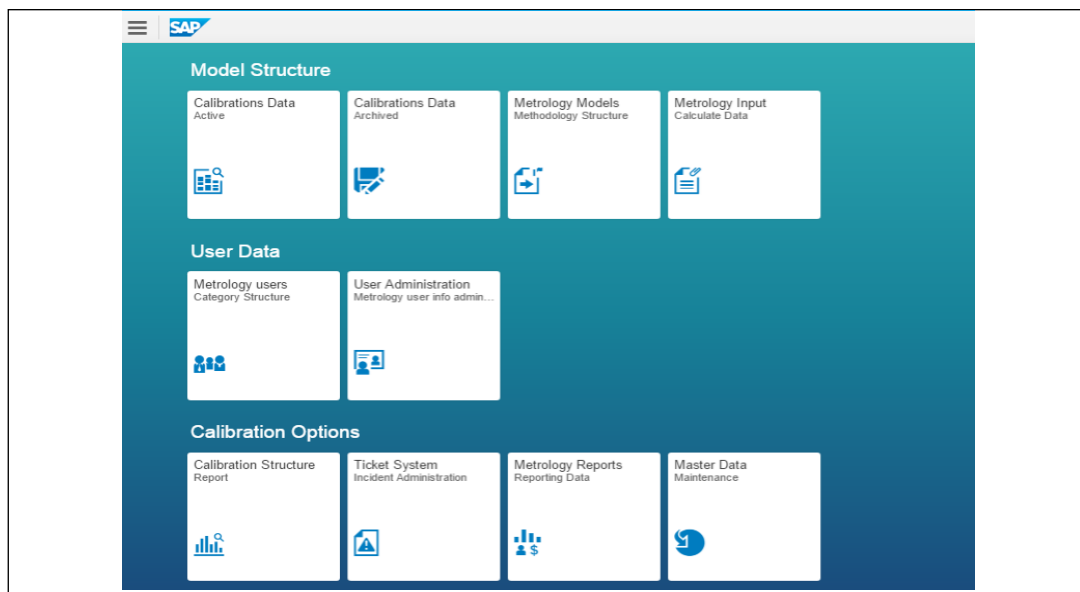


Fig. 6 SAP Fiori interface for CRT tool

bigger than the value described before (BRML, 2007).

The underlying principles for CRT tool as a software tool/application were metrology rules, standard ones, all metrology papers, guiding metrology principles (according with BRML standards and guidelines). After the data are collected from the territory, are synthesized, grouped, and a mathematical computation is used for all data, in order to obtain good results, according with the imposed rules. A calibration content (table) is created for each tank/reservoir when the measurement is started, based on resulted data from the entire area (tank) which is in scope for this calibration. The reference temperature for each collected value (partial capacity), will be 20 Celsius degrees (BRML (2007)). For our case study, the mathematical computation based on heights measurements, linear interpolation, outside temperature influence regarding fluid expansion effect, and relation between volume and water mass. The data from calibration certificate are taken into account (BRML (2007)).

### 3. METROLOGY IMPLEMENTATION CONCEPT – DESIGNED WITH SAP FIORI

When we started to design our software, inside SAP, we already knew that SAP it's the leader in the world, is installed in our company and we can integrate our processes (e-metrology processes) in the oil and gas company of which we are part. Our processes (e-metrology part) have to be part of processes which cover the legal and engineering for demand management department. With the transformation to SAP Fiori, we tried and we succeeded to move our interface with our application/software for our colleagues to mobility, to tablets or smart mobiles. We focused on processes, like SAP does day by day, in all companies where is installed, knowing that the SAP (System and Applications, Products) (Goebels and all., 2016) is the largest ERP in the world and knowing that this software is created base on client/server architecture, so as a conclusion we start from collecting, designing, planning processes and finished with the new interface, mobility one (Orosz, 2011). Our main application is written using

ABAP, Web Dynpro (WD), SAP Fiori, HTML5, Javascript, this means that will arise a lot of advantages for SAP configuration (landscapes - environments), as there are described below:

- the tool (WD) can support all phases for development (design, development, implementation, support, etc.);
- the professional Web UI's (Web User Interface) are developed using the discussed model for our business application / software
- layout data and business data are clear separated
- easy modelling our WD software / application
- it's easy to use the possibility to define a new model for PC or smart phone
- regarding the implementation time, it's clear that this time will be reduced
- the WD concept supports a structured process design
- HTML 5 is easy to be used, even Javascript are generate automated by the tool.

For our colleagues (E&P and Marketing divisions) with the value of the SAP Fiori interface, we add more value regarding user interface (new user experience (UX) - as is described in the SAP methodology), this means that SAP Fiori in combination with HTML5 and Javascript, comes with a lot of applications that are used in structured business functions like how we approve our work, in financial applications, calculation applications and a lot of self-service applications in metrology area, like our designed application – CRT tool.

SAP comes with some principles for SAP Fiori interface, principles which have to be used in our development, some of them, we will describe them in the below context: everything is based on well-defined roles; it is adaptable to changes; everything is simple so everything is fast (functions, tasks, activities) (Gahm and all., 2016), (Adams, 2016), (Prewett and Pytel, (2016); we have the same UX experience across the system, whether you need to see/read/write a metrology ticket (Fig. 9), review your



Fig. 7 Old and new CRT tool interface using SAP Fiori

latest KPI's or manage situations; everything are intuitive, easy to use, our work is delightful with Fiori Launchpad (Fig. 6).

#### 4. NEW APPLICATION CONCEPT / IMPLEMENTATION WITH SAP FIORI

In the Demand Management team from E&P or Marketing divisions (inside oil and gas companies,) with dedicate structures - metrology structure, calibrations are used every year in order to have all the documents safe for possible checks, regarding the metrology activity (legal papers coming from BRML). These calibrations are part of the activities which are necessary to maintain our fixed assets (horizontal / vertical tanks, different types of small reservoirs, underground tank, etc.) which are part of legality controls from the authorities from our country.

When we started talking about the CRT tool, we first put together what we knew about metrology, principles, and practical work with what colleagues in E & P and Marketing had collected from past calibrations.

combine, SAPUI5, HTML5, Javascript and CSS into toolkit - anyway they are the latest technology) in order to build applications (mobile or desktop ones), the best advantage is that we can run this on a browser. Our target was to modify our software application in order to be used as a web application on our platform SAP ERP. Our advantages, with these modifications, was that our tool can be rendered in two cases: on the desktop or on the mobile smartphones devices (any device for any platforms). This new implementation was considered a success because of this new advantage – mobility which not restricts the capability to see, add, modify data, so, everything can be done everywhere, with clear rules from BRML legal institution and existing procedures in our company. Our new modifications / development will help the users, using mobility, to access the application via web / mobility. The CRT tool content, the dates contained in this application, will be seen by end-users, via SAP Portal and SAP Fiori interface, using smart mobile

from the oil and gas sectors and will be stored using specific forms, in concordance with BRML rules. The

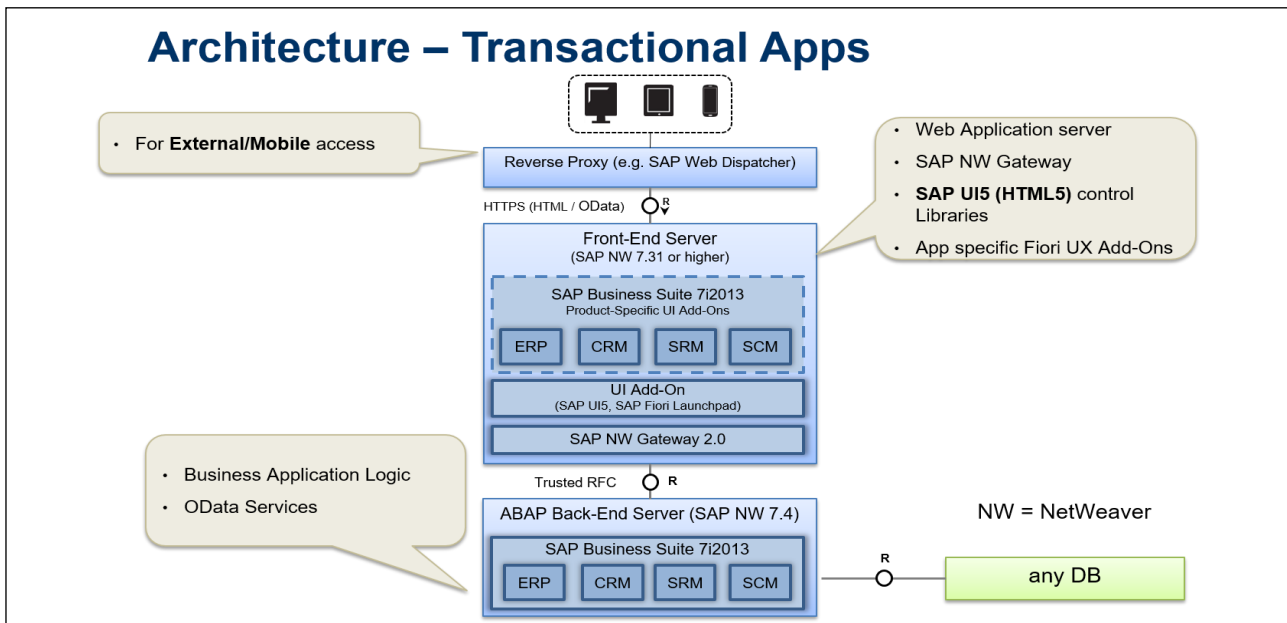


Fig. 8 SAP Fiori architecture – interface for CRT tool

Our discussions were relevant to us as IT, meaning we had to build a collapsible structure subsequently by other technologies so software CRT application (we done our programming language using ABAP - Advanced Business Application Programming – used for SAP) can be remodelled so that it can keep up with everything that is new. Now, starting with this year we have interfaced the application created with SAP Fiori in order to help our colleagues to use mobility with all his existing features.

In the Fig. 8 we have designed the architecture principle of SAP Fiori / OData which is used for our application, identifying SAP ERP as a most important data sender and importer from the external mobility interface. SAPUI5 collection of libraries are the most relevant technical support for SAP Fiori and is used by our developers (he

benefits for our colleagues from the E&P and Marketing divisions, using our software application, are multiple, they have the opportunity to have in one single database all their metrological calculations, accurate, visible on-line.

Multiple tested algorithms for calibrations are used in order to be on legal side, according with our legislation from BRML (Banta and al., 2014).

Our tool contains several proved methods for calibration and together with all the technical data that we have available, we can upload with different tools (excel, text delimited, csv, etc.) a lot of calibration data from the territory, with tablets, smart phones, etc. from the oil, gas, filling stations sectors (in the territory, manual measurements are place - can be added in the CRT tool manually or automated).



## 6. CONCLUSION

Our research executed in concordance with this article, can demonstrate that for this part of industry, oil and gas, the metrology architecture can be adapted and can be attached with an ERP which is installed in this area of business. The reason for developing this software tool, in the existing SAP ERP, demonstrate that our application can be assimilate with a rigorous, fully and auditable tool and can be used for producing and storing data for legal perspective. More than that, every year, we have to improve our tool, based on SAP innovation, with this paper we add the part of interfaces with mobility zone - SAP Fiori. With this innovation our application can be used inside and outside of our company - starting from HQ - and extended to our all country - using mobility architecture.

Our software CRT application / tool presented are business oriented, in the metrology area, and is designed to help our colleagues in order to collect, calculate, store the needed data for metrological calculations for reservoirs, regardless of their type, for Exploration & Production and Marketing (filling stations) areas. The main scope for CRT tool is to unify the way of working in the company, in this area, of legal metrology management for tanks and reservoirs belonging to oil and gas business environment. CRT tool when was designed - the main scope was - to collect, to store technical data and components (structured one) for used reservoirs (oil and gas reservoirs) for metrological calculation / store data reasons - the metrological data results are now unified, the same methods and rules are used for all calibrations (three models are used: dispatcher model, body-leasing model, calibration given outside (fixed price)). In the existing integrated ERP systems, with this tool, the originators developed and adapted a software system for monitoring, reporting and storing metrology data and they expanded the usage of the tool for mobility.

The CRT tool / application was integrated in SAP (System and Application, Products) and was developed in ABAP (Advanced Business Application Programming) programming environment, HTML5 and Javascript, now the application is integrated with SAP Fiori for mobility reason. We used a WebDynpro tool according with the intention to move the utility of the application to web.

## REFERENCES

- Adams, DJ. (2016). *SAP Fiori and SAPUI5: Debugging the User Interface*. SAP Press
- Antolovic, M. (2014). *Getting Started with SAPUI5*. SAP Press
- Banta, V.C., Cojocaru, D. and Tanasie, R.T. (2012). A Software Application for the Gas Transport and Distribution Management, *Annals of the University of Craiova, Series: Automation, Computers, Electronics and Mechatronics*, Vol. 10 (37), No. 2, 2012, ISSN 1841-0626, pages 1-6.
- Banta, V.C. and Cojocaru, D. (2013). Development Center Tool a Software Application for Change Request Management, *17th International Conference on System Theory, Control and Computing Joint Conference SINTES 17, SACCS 13, SIMSIS 17*, ISBN 978-1-4799-2228-4, ISBN 978-1-4799-2227-7, p42-47, 11 - 13 October 2013, Sinaia, Romania.
- Banta, V.C. and Cojocaru, D. (2014). Calibration Oil Reservoirs - A Software Application for Metrology, *International Conference on System Theory, Control and Computing ICSTCC 2014, SINTES 18, SACCS 14, SIMSIS 18*, October 2014, Sinaia, Romania.
- Banta, V.C., Cojocaru, D. , Moisescu, M.A. and Sacala, I.S. (2014). Release Management Tool - A Software Application for Release and Deployment Management, *the 5th edition of the IACSIT / SCIEI / UASTRO International Conference on Optimization of the Smart systems and their Application ICMERA*, 24-27 October 2014, Bucharest, Romania.
- Banta, V.C., Cojocaru, D. , Moisescu, M.A. and Sacala, I.S. (2014). Software Design for Oil Industry Metrology Systems. *Studies in Informatics and Control Journal, ICI Bucharest 2014*, Romania, November, SIC-4/2014.
- Bavaraju, A. (2016). *SAP Fiori Implementation and Development*. SAP Press.
- Bönnen, C., Drees, V., Fischer, A., Heinz, L., Strothmann, K. (2016). *SAP Gateway and OData*. SAP Press
- BRML, PIV 017-05-02. Metrological procedure for liquid storage tanks, Edition 1, Revision 0 / PV 017-05-01-07 "Verification procedure for liquid storage tanks".
- Chen, S.G.G. and Lin, Y.K/K. (2008). Performance analysis for Enterprise Resource Planning systems. In *Industrial Engineering and Engineering Management, IEEM 2008, IEE International Conference*, pp. 63-67.
- Gahm, H., Schneider, Th., Swanepoel, C., Westenberger, E. (2016). *ABAP Development for SAP HANA*. SAP Press
- Goebels, C., Nepraunig, D., Seidel, T. (2016). *SAPUI5 - The Comprehensive Guide*. SAP Press.
- Jardim-Goncalves, R., Grilo, A., Agostinho, C., Lampathaki, F. and Charalabidis, Y. (2012) Systematisation of Interoperability Body of Knowledge: the foundation for Enterprise Interoperability as a science. *Enterprise Information Systems*, vol. 6, no. 3, pp. 1-26.
- Keller, E.L.. Lessons Learned, *Manufacturing Systems*, Vol. 17, Issue 11, pp. 44-50.
- Leu, J.D. and Huang, L.T. (2009). Logistics planning of the IC manufacturing industry: A method based on the SAP-APO, *Computers & Industrial Engineering, CIE 2009, Intel. Conf.*, pp. 760 – 766.
- Lin, C.C. and Shih, D.H. (2009). Information System Reengineering for Enterprise Resource Planning as Businesses Adapting to the E-business Era. In *Software Engineering, WCSE 2009, WRI World Congress on*, Vol. 3, pp.222-226.
- Orosz, T. (2011). Analysis of SAP Development tools and methods. In *Intelligent Engineering Systems (INES), 15th IEEE International Conference*. pp. 439 – 443.
- Peter, M. and Pohl, T. (2009). *Developing Enterprise Services for SAP*. Galileo Press.
- Prewett, G., Pytel, M. (2016). *Implementing SAP Fiori Security*. SAP Press
- Szirtes, T., Rivlin, A. (2015). *Implementing SAP Fiori Launchpad*. SAP Press





## AUTHOR INDEX

Faiq BAJI	20
Viorel Costin BANȚA	40
Laviniu Aurelian BĂDULESCU	15
George Cristian CĂLUGARU	34
Dorian COJOCARU	40
Elena Andreea DĂNIȘOR	34
Mihai MOCANU	20
Anca PURCARU	5
Dorina PURCARU	5
Ionuț Cristian RESCEANU	34
Traian-Titi ȘERBAN	28